Alkalinity generation from carbonate weathering in a silicate-dominated headwater catchment at Iskorasfjellet, northern Norway

Nele Lehmann[1,2,3], Hugues Lantuit[2,4], Michael Ernst Böttcher[5,6,7], Jens Hartmann[8], Antje Eulenburg[2], Helmuth Thomas[1,3]

[1]Institute of Carbon Cycles, Helmholtz-Zentrum Hereon, Geesthacht, D-21502, Germany
[2]Alfred Wegener Institute Helmholtz Centre for Polar and Marine Research, Potsdam, D-14473, Germany
[3]Institute for Chemistry and Biology of the Marine Environment (ICBM), University of Oldenburg, Oldenburg, D-26129, Germany
[4]Institute for Geosciences, University of Potsdam, Potsdam, D-14476, Germany
[5]Geochemistry and Isotope Biogeochemistry, Leibniz Institute for Baltic Sea Research (IOW), Warnemünde, D-18119, Germany
[6] Marine Geochemistry, University of Greifswald, Greifswald, D-17489, Germany
[7]Interdisciplinary Faculty, University of Rostock, Rostock, D-18059, Germany
[8]Institute for Geology, Center for Earth System Research and Sustainability, University Hamburg, Hamburg, D-20146, Germany

Correspondence to: Nele Lehmann (nele.lehmann@hereon.de) and Helmuth Thomas (helmuth.thomas@hereon.de)

Abstract. The weathering rate of carbonate minerals is several orders of magnitude higher than for silicate minerals. Therefore, small amounts of carbonate minerals have the potential to control the dissolved weathering loads in silicate-dominated catchments. Both weathering processes produce alkalinity under the consumption of CO_2. Given that only alkalinity generation from silicate weathering is thought to be a long-term sink for CO_2, a misattributed weathering source could lead to incorrect conclusions about long- and short-term CO_2 fixation. In this study, we aimed to identify the weathering sources responsible for alkalinity generation and CO_2 fixation across watershed scales in a degrading permafrost landscape in northern Norway, 68.7 – 70.5 °N, and on a temporal scale, in a subarctic headwater catchment on the mountainside of Iskorasfjellet, characterized by sporadic permafrost and underlain mainly by silicates as the alkalinity-bearing lithology. By analysing total alkalinity (AT) and dissolved inorganic carbon (DIC) concentrations, as well as the stable isotope signature of the latter (δ^{13}C-DIC) in conjunction with dissolved cation and anion loads, we found that AT was almost entirely derived from weathering of the sparse carbonate minerals. We propose that in the headwater catchment, the riparian zone is a hotspot area of AT generation and release due to its enhanced hydrological connectivity, and that the weathering load contribution from the uphill catchment is limited by insufficient contact time of weathering agent and weatherable material. By using stable water isotopes, it was possible to explain temporal variations in AT concentrations following a precipitation event due to surface runoff. In addition to carbonic acid, sulphuric acid, probably originating from ~~pyrite~~ oxidation of pyrite or reduced sulphur in wetlands or from acid deposition, is shown to be a potential corrosive reactant. An increased proportion of sulphuric acid as a potential weathering agent may have resulted in a decrease in AT. Therefore, carbonate weathering in the studied area should be considered not only as a short-term CO_2 sink, but also as a potential CO_2 source. Finally, we found that AT increased with

decreasing permafrost probability, and attributed this relation to an increased water storage capacity associated with increasing contact of weathering agent and rock surfaces, and enhanced microbial activity. As both soil respiration and permafrost thaw are expected to increase with climate change, increasing the availability of weathering agent in the form of CO_2 and water storage capacity, respectively, we suggest that future weathering rates and alkalinity generation will increase concomitantly in

40   the study area.

1 Introduction

Weathering of silicate rocks is thought to be the long-term sink (millions of years) for atmospheric CO_2 (Berner et al., 1983; Garrels and Berner, 1983). Weathering of both carbonate and silicate rocks consumes atmospheric/soil CO_2 and increases the alkalinity of the ocean. ~~While alkalinity generation from weathering of calcium silicates contributes to the long-term~~

45   ~~drawdown of CO_2 via the precipitation of carbonates in the ocean and thus the return of carbon to the lithosphere, the alkalinity generation from weathering of carbonate rocks does not have such an impact on these timescales.~~ Carbonate and silicate weathering are thought to be~~Carbonate weathering is thought to~~ in equilibrium with marine calcification over shorter time-scales (<10,000 years; Zeebe and Westbroek (2003)). Beyond the calcium carbonate compensation time, only silicate weathering acts as a long-term sink for atmospheric CO_2, while carbonate weathering acts CO_2-neutral (Berner et al., 1983;

50   Garrels and Berner, 1983). Since only alkalinity produced by silicate weathering is thought to be a long-term CO_2 sink, a misattributed weathering source could lead to incorrect conclusions about long- and short-term CO_2 fixation. Global estimates (Gaillardet et al., 1999; Amiotte Suchet et al., 2003; Hartmann et al., 2009) attribute 49-63% of CO_2 consumption by terrestrial weathering to silicate rocks, the remainder to carbonate rocks. These studies rely on lithological maps and bulk river chemistry data used to infer whether CO_2 consumption is due to silicate or carbonate weathering. However, some case and regional

55   studies (Blum et al., 1998; White et al., 1999; Jacobson et al., 2002; Jacobson et al., 2003; Oliver et al., 2003; White et al., 2005; Moore et al., 2013; Jacobson et al., 2015) indicate that the global calculations relying on bulk river chemistry data may overestimate silicate weathering. Hartmann (2009) pointed out that interpretation of the molar ratio of Ca^{2+}/Na^+ may lead to incorrect attribution of CO_2 drawdown to silicate weathering in predominantly silicate areas, which should instead be attributed to the weathering of accessory carbonate minerals. H~~e~~artmann (2009) calculated trace carbonate contribution for igneous rocks

60   and silicate sediments for the Japanese Archipelago, and later applied the developed multilithological regression method globally (Hartmann et al., 2009). Especially silicate-dominated regions that are physically active, e.g., during glaciation and tectonism, or that exhibit early stages of weathering due to freshly deposited material or recent deglaciation or uplift, ~~which are physically active or show early stages of weathering (e.g. during and following periods of glaciation and tectonism)~~ show high weathering loads of accessory carbonate minerals such as calcite, aragonite and dolomite (Jacobson et al., 2002; Jacobson

65   et al., 2003; White et al., 1999; Oliver et al., 2003; White et al., 2005; Moore et al., 2013; Jacobson et al., 2015). The weathering rate of carbonates is several orders of magnitude faster than the ~~one~~ weathering rate of silicates (Lasaga, 1984; Stallard and

Formatiert: Tiefgestellt

Formatiert: Tiefgestellt
Formatiert: Tiefgestellt
Formatiert: Tiefgestellt
Formatiert: Tiefgestellt

Edmond, 1987; Jacobson et al., 2003), thus dissolved inorganic carbon (DIC) is often controlled by carbonates (Liu et al., 2018).

70 DIC is composed of CO_2^* (i.e., the sum of dissolved CO_2 and H_2CO_3), HCO_3^- and CO_3^{2-}, with the relative proportion of the DIC species depending on alkalinity and environmental conditions such as temperature. In fresh water, total alkalinity (AT), or acid-neutralizing capacity, is mainly composed of carbonate alkalinity (i.e., HCO_3^- and CO_3^{2-}) and, to a lesser extent, hydroxide ions (OH^-). At pH values between 7 and 9, the alkalinity concentration is approximately equal to the HCO_3^- concentration (~95% of the carbon in the water is in the form of HCO_3^-), as the equilibrium between CO_2^*, HCO_3^- and CO_3^{2-}

75 in this pH range is strongly in favour of HCO_3^- (Stumm and Morgan, 1981). Alkalinity in the form of HCO_3^- is produced from the weathering of carbonate minerals (shown here for calcite) under the consumption of one equivalent of atmospheric and/or soil CO_2 as follows:

$$CaCO_3 + CO_2 + H_2O \leftrightarrow Ca^{2+} + 2\,HCO_3^- \qquad (1)$$

Assuming that the weathering agent is not carbonic acid, but other inorganic acids such as sulphuric and nitric acid, and

80 carbonate is not present in excess but as accessory carbonates (Appelo et al., 1998), carbonate weathering (shown here for calcite weathering with sulphuric acid) releases CO_2, thereby increasing the DIC concentration, but not contributing to alkalinity generation (Berner and Berner, 1987; Marx et al., 2017a; Liu et al., 2018):

$$CaCO_3 + H_2SO_4 \leftrightarrow Ca^{2+} + SO_4^{2-} + H_2O + CO_2 \qquad (2)$$

Sulphuric acid can be generated from the dissolution of sulphate-containing minerals, such as gypsum, or the oxidation of

85 sulphide minerals, such as pyrite, or the oxidation of reduced sulphur stores in wetlands (including permafrost). Furthermore, both sulphuric and nitric acid can be brought into the soil via acid deposition rain. Finally, nitric acid can also be produced from the oxidation of ammonium fertilizers or through nitrification of reduced nitrogen stores in wetlands (Marx et al., 2017a; Li et al., 2010).

While in carbonic acid induced carbonate weathering only one of the two equivalents of HCO_3^- is derived from atmospheric

90 and/or soil CO_2, in silicate weathering all HCO_3^- originates from CO_2 (shown here for anorthite weathering, one of the three major types of feldspar):

$$CaAl_2Si_2O_8 + 2\,CO_2 + 3\,H_2O \rightarrow Al_2Si_2O_5(OH)_4 + Ca^{2+} + 2\,HCO_3^- \qquad (3)$$
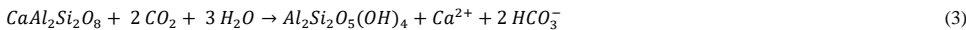
When silicates are weathered by non-carbon based acids, neither DIC nor AT is generated (shown here for anorthite weathering with sulphuric acid):

95 $$CaAl_2Si_2O_8 + H_2SO_4 \rightarrow 2\,AlOOH + Ca^{2+} + SO_4^{2-} + 2\,SiO_2 \qquad (4)$$
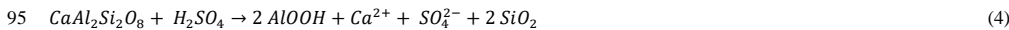
A valuable tool to distinguish between the sources of DIC in streams is the stable isotope composition of DIC, δ^{13}C-DIC (Deines et al., 1974; Böttcher, 1999), which varies across a wide range, typically from +5‰ to -35‰ (Campeau et al., 2017). In addition to the above mentioned geogenic sources, DIC is also governed by biogenic sources, CO_2 evasion, and in-stream processes (Kempe, 1982; Campeau et al., 2017). Biogenic DIC originates from autotrophic respiration, heterotrophic

100 respiration, or organic matter mineralization (e.g., photo-oxidation of dissolved organic carbon (DOC)). In regions dominated

by C3 plant vegetation, this biogenic DIC has a typical $\delta^{13}C$ value of about -27‰ (O'Leary, 1988). When measured in soil solution, this value typically increases by 1-4‰, as dissolution and gas exchange across the soil-atmosphere interphase take place (Cerling et al., 1991; Davidson, 1995; Amundson et al., 1998). When carbonate minerals, which have a typical $\delta^{13}C$ value of about 0‰ (Hoefs, 1973; Land, 1980), are weathered by soil respired dissolved CO_2 (about -24‰), the final DIC is at saturation with carbonate minerals and is characterized by an isotopic composition of about -12‰, considering evolution under conditions closed with reference to a CO_2 gas phase in C3 vegetation-dominated catchments (Deines et al., 1974). C4-type of vegetation leads to shift towards heavier stable isotope values (Deines et al., 1974). When the weathering takes place by other inorganic acids, the resulting $\delta^{13}C$-DIC can even turn more positive to about -6 to -1‰ (Schaefer and Usdowski, 1987, 1992; Michaelis, 1992; Zolkos et al., 2020) and reach under extreme conditions the $\delta^{13}C$ value of carbonate minerals of about 0‰ (Lehn et al., 2017). The actual isotope composition of DIC depends also on the boundary conditions (presence of biogenic CO_2) during the groundwater evolution (Deines et al., 1974; Schaefer and Usdowski, 1987, 1992; Böttcher, 1999). DIC generated from carbonic acid induced silicate weathering has a typical $\delta^{13}C$ value of about -24‰, as soil CO_2 is the dominant source for DIC (Lehn et al., 2017; Purkamo et al., 2022) and fractionation between the aqueous and gas phase is small at low pH values (Deines et al., 1974).

When CO_2 is degassed from the stream due to supersaturation, which is especially prominent in headwater catchments (Michaelis et al., 1985; Marx et al., 2017a), the remaining stream water DIC is enriched in ^{13}C (Michaelis et al., 1985; Liu and Han, 2020). Equilibrium exchange fractionation between stream DIC and atmospheric CO_2, which has a typical $\delta^{13}C$ value of about -8‰ (Trolier et al., 1996), has the same effect on stream $\delta^{13}C$-DIC as CO_2 outgassing (Michaelis et al., 1985; Liu and Han, 2020).

Finally, the $\delta^{13}C$-DIC values on flowing surface waters may also be influenced by in situ biogeochemical processes such as biological respiration, DOC photo-oxidation, photosynthesis, mixing with groundwaters, and anaerobic metabolism (Campeau et al., 2017).

The general controls on chemical weathering are the availability of weatherable minerals, mainly provided by physical weathering of regolith, and the supply of weathering agents, i.e., acids (Raymond and Hamilton, 2018). In addition to carbonic acid, the main source of terrestrial weathering, organic acids from vegetation (mainly carboxylic acids) and strong inorganic acids (mainly sulphuric and nitric acid, derived from the oxidation of sulfides and ammonium, respectively; Raymond and Hamilton, 2018) drive the weathering reactions. However, to the best of our knowledge, there is not any study showing the effect of DOC on the weathering reaction. Further, to generate the soluble weathering products, favorable conditions such as high temperatures, abundant moisture and high contact of mineral surfaces with water should prevail. Lastly, the hydrological transport of these solutes out of the weathering zone is another controlling factor (Raymond and Hamilton, 2018).

Feedback between the Earth's carbon cycle and terrestrial weathering was originally thought to be slow, and CO_2 consumption by terrestrial weathering to be at steady-state since pre-industrial times (Walker et al., 1981; Berner et al., 1983). However, a global study (Goll et al., 2014) reported increased CO_2 consumption since 1850, and regional studies (Li et al., 2008; Gislason

135 et al., 2009; Raymond et al., 2008; Drake et al., 2018; Macpherson et al., 2019) found an increase in riverine alkalinity over the last decades and related this to changes in temperature, precipitation, vegetation, availability of acids, liming, or hydrologic flow conditions. Thawing permafrost in cold regions was also assumed, too; thereby advocating for a possibly rapid (decadal) feedback between climate and land-use change and riverine alkalinity generation upon terrestrial weathering. Especially carbonate weathering was found to strongly respond be very responsive to contemporary environmental changes (Michaelis,

140 1992; Zeng et al., 2019). Besides the tropical region, northern high latitudes are expected in the future to experience enhanced carbonate weathering and thus a higher carbon-sink function due to increased soil CO_2 partial pressures and temperatures (Zeng et al., 2022). The drivers of the increased soil pCO_2 are increased ecosystem productivity and soil respiration (Zeng et al., 2022). The aquifers and soils of Fennoscandia, however, are mainly composed of non-carbonate rocks (O'Nions et al., 1970; Hartmann and Moosdorf, 2012; Zeng et al., 2022), and therefore, a response in terms of CO_2 sequestration through

145 weathering on environmental changes might be expected to be slow (Moosdorf et al., 2011).

Climate change is particularly accelerated in the Arctic, as reflected in the annually averaged near-surface air temperature, which increased by 0.71°C per decade from 1979 to 2021, nearly four times faster than the global average (Rantanen et al., 2022). This rapid warming simultaneously affects permafrost, hydrology, soil carbon stores, and surface vegetation, with all of these processes having the potential to alter the generation of alkalinity (Drake et al., 2018). Permafrost thaw causes the

150 Arctic terrestrial freshwater system to increase its connectivity between surface waters and deeper groundwater pathways (Striegl et al., 2005; Walvoord and Striegl, 2007) and may ultimately move from a surface water-dominated to a groundwater-dominated system (Frey and McClelland, 2009). Thawed soils allow for longer residence times of infiltrating surface water, thereby facilitating more contact with unweathered mineral surfaces and additional mixing with mineral-rich groundwater, resulting in higher alkalinity fluxes (Drake et al., 2018). So far, studies about fast feedback between alkalinity generation from

155 rock weathering and climate change in northern high latitudes have investigated the impact of a varying glacial cover (Gislason et al., 2009) or retrogressive thaw slumps (Zolkos et al., 2020) or focused on large Arctic river systems (Drake et al., 2018) and on subcatchments of the circumboreal (Tank et al., 2012). An in-depth study of the weathering processes in catchments of the silicate-rich Fennoscandian Shield in northern Norway, potentially influenced by a changing climate, which could lead to an enhanced alkalinity generation, is still missing.

160

Our aim in the present study is to identify the weathering pathways responsible for alkalinity generation in a small subarctic catchment on the mountainside of Iskorasfjellet in northern Norway mainly dominated by silicate minerals and characterized by sporadic permafrost during early fall of 2020. In particular, we aimed at distinguishing between different weathering agents (dissolved CO_2 vs. other acids) and different source minerals (silicate vs. carbonate) under different environmental forcings,

165 thereby analysing the potential factors for CO_2 drawdown. In addition to the detailed analysis of the Gaskabohki watershed at Iskorasfjellet, we extended the investigation of controlling factors on alkalinity generation to several other catchments, some of which stretch as far as the Barents Sea with varying extent of permafrost, in order to establish broader implications and evaluate how climate change might provide feedback for CO_2 sequestration in this subarctic region.

2 Materials and methods

2.1 Study site

The Gaskabohki watershed (catchment area = 0.7 km^2) is a headwater catchment located on the mountain slope of Iskorasfjellet, Karasjok Municipality, northern Norway (Fig. 1). Iskorasfjellet is situated inland on the Finnmarksvidda plateau (300-500 m above mean sea level (amsl)), with local peaks rising above 600 m amsl), which borders Finland to the south and east. The Finnmarksvidda plateau was completely covered by the Fennoscandian ice sheet during the last glaciation (Olsen et al., 2013). In addition to being covered by the Fennoscandian ice sheet with an ice dome zone over Finland during the last stadial, the Finnmarksvidda was also covered by the Scandinavian ice sheets which grew from the mountainous area of northwest Sweden and from centers along the Caledonian mountain range in Norway during the Middle and Early Weichselian (Olsen, 1988; Olsen et al., 2013). The Finnmarksvidda plateau was completely ice-covered during the Pleistocene glaciations. Due to glacial activity, ground-moraine, glaciofluvial, and glaciolacustrine sediments were accumulated on the surface geology (Sollid et al., 1973). Various soil types are present on the Finnmarksvidda plateau: podzols with a thin to medium bleached layer, swamp soils, lithosols, rankerlike soils and brown earths (Lag, 1983). Iskorasfjellet was deglaciated ~10,900-10,800 cal. yr BP (Stroeven et al., 2016). The Gaskabohki catchment is underlain by quartzite and arkose, in places with layers of different shales (NGU, 2022). Therefore, the alkalinity-bearing lithology is dominated by feldspar, with minor contribution of calcite within the shales. Just before the outlet, however, a small area of partly calcareous quartz feldspar shale (0.5% areal proportion of the entire catchment area) underlies the catchment. This area coincides with a wider riparian zone (Fig. 1d). Besides the main channel, drainage gullies are present which were dried out at the time of sampling in the fall.
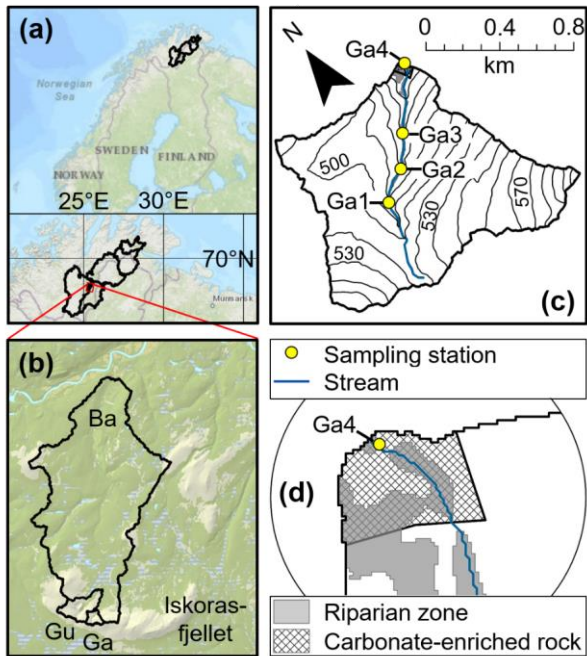
Figure 1: Study area. (a) Location of all studied basins in Fennoscandia. Background map from Esri, HERE, Garmin, FAO, NOAA, USGS (ESRI, 2022). **(b)** Zoom on the study area at Iskorasfjellet with the Bahkiljohka (Ba), Guovzilbohki (Gu) and Gaskabohki (Ga) catchments. Background map is the ArcGis web map "Topografisk Norgeskart" (ESRI, 2022). **(c)** Zoom on the Gaskabohki headwater catchment with sampling stations Ga1 – Ga4 (Gaskabohki 1 – Gaskabohki 4). Contour interval = 10 m. **(d)** Zoom on the outlet of the Gaskabohki catchment with the wider riparian zone overlapping with an area of partly calcareous quartz feldspar shale (carbonate-enriched rock).

From the top of the mountain at 644 m amsl., the landscape slopes down (~3% slope) to the Iskoras peat plateau at ~380 m amsl. The peat began to form around 9,800 cal. year B.P. in the form of wet fens, which were prevalent during most of the Holocene. Dry surface conditions associated with permafrost peat plateau aggradation developed around 950–100 cal. year B.P., probably caused by the Little Ice Age cooling (Kjellman et al., 2018).

The Iskoras peat plateau is enclosed by the Bahkiljohka catchment (catchment area = 78 km^2; Fig. 1b), which is underlain by an increased proportion of partly calcareous quartz feldspar shale (up to 34% of areal carbonate extent (NGU, 2022)) when compared to the Gaskabohki catchment (0.5%). From Iskorasfjellet, the sampling area stretches out further northeast, following the larger rivers Karasjohka and Tanaelva, until the Tanafjord. While the Bahkiljohka catchment is characterized by isolated patches of permafrost (catchment average permafrost probability = 0.04), the Gaskabohki watershed as well as the rest of the

studied area show sporadic permafrost (catchment average permafrost probability = 0.10-0.17) (Obu et al., 2019). Permafrost probability is defined as the fraction of ensemble members (N = 200 for each 1 km^2 grid cell) with a mean annual ground

205 temperature of 0°C or lower (Obu et al., 2019). Tundra vegetation (e.g., lichen crusts, *Betula* shrubs and *Empetrum nigrum* ssp. *hermaphroditum*) dominates at Iskorasfjellet. Below an elevation of ~570 m amsl, mountain birch (*Betula pubescens* ssp. *czerepanovii*) forest is also present.

The climate of Finnmarksvidda is continental. For the last six years (September 2014 - August 2020, longest continuous record at Iskorasfjellet), the mean summer (June-July-August) and winter (December-January-February) air temperatures were 8.7 °C

210 and -9.3 °C, respectively (measured at the meteorological station at Iskorasfjellet, 591 m amsl, SN97710; (Seklima, 2020)). Compared to the air temperature normal (1961-1990), temperatures increased by 0.2 °C and 4.2 °C, respectively. Mean monthly precipitation sums during the summer and winter for the last six years were 66 mm and 38 mm, which correspond to 117% and 237% of the monthly precipitation sums of the climate normal, respectively. The annual precipitation averaged over the last six years, from September 2017 – August 2020, was 492 mm (measured at the meteorological station in Karasjok,

215 131 m amsl, SN97251, 20 km from Iskorasfjellet; (Seklima, 2020)). The mean daily snow depth during the snow season (October – May) was 29 cm (measured at the meteorological station at Iskorasfjellet, 591 m amsl, SN97710; (Seklima, 2020)). During the sampling campaign in fall 2020, a precipitation sum of 7 mm was measured, which is about half of what was recorded over the same period averaged over the six years prior to sampling (Seklima, 2020). Thus, the fall of 2020 was comparatively dry. There was no snowfall and the mean daily air temperature averaged over the sampling period was 3.9 °C,

220 which is ~2.7 °C higher than during the same fall period 2014-2019 (Seklima, 2020).

2.2 Water sampling

From September 22nd to October 6th 2020, we collected water samples daily from the outlet of the Gaskabohki catchment (Ga; Fig. 1b-d) to investigate how DIC and AT may change under different environmental forcing (changing precipitation and temperature). We further sampled weekly (3x) at three stations upstream of the outlet to track the changes of the carbonate

225 system with distance from the spring. All data can be accessed at https://doi.org/10.1594/PANGAEA.952905. Besides this temporal examination, we also expanded the investigation spatially, by and collecteding water samples from seven further catchments (Fig. 1a). These catchments included the Guovzilbohki headwater catchment (Gu; Fig. 1b), which shows similar topographic properties as the adjacent Gaskabohki watershed, but a higher carbonate-to-silicate bedrock ratio.; the Bahkiljohka catchment (Ba; Fig. 1b) which is characterized by the lowest permafrost probability.; and five larger catchments (catchment

230 area = 4,900-15,000 km^2). In that way, we were able to investigate further controlling factors (catchment area, roughness, permafrost probability, peatland cover, EVI (mean enhanced vegetation index), and bedrock lithology) on alkalinity generation.

At all sampling sites, we collected water samples for DIC and AT, δ^{13}C-DIC, major elements, and stable water isotopes (δ^{18}O-H$_2$O and δ^2H-H$_2$O). For DIC and AT analysis, we collected the river water directly into 300-mL BOD bottles, added 300 μL

235 of saturated mercury chloride solution and sealed the bottles with ground-glass stoppers, Apiezon type M grease and plastic

caps (no-head space). For δ^{13}C-DIC analysis, the solution was membrane-filtered (0.45 μm pore widths) into 12-mL glass vials, 10 μL of saturated mercury chloride solution were added, and the vials were sealed with a septum without head space. For cation measurements, we filtered the surface water (0.45 μm pore widths) into 50 mL acid-washed tubes and acidified the samples with 50 μL of concentrated trace metal-grade HNO_3. For anion measurements, we filtered (0.45 μm pore widths) the samples into 15 mL tubes, from which we later took an aliquot (~1.5 mL) for stable water isotope analysis. All samples were stored in the dark at ambient temperature (~1-10 °C). We measured stream temperature and electric conductivity using a precalibrated WTW Multi3430 with IDS TetraCon 925, and turbidity using a precalibrated HACH 2100Qis. Finally, at the outlet of the Gaskabohki catchment, we performed a discharge measurement once a day, at the same time as taking the water samples, by recording stream velocity using a Marsh-McBirney Model 2000 Flo-Mate portable flow meter at increments equal to ~10% of the stream width. By measuring the corresponding stream depth, we were able to calculate stream discharge from the product of stream velocity and cross-sectional area.

2.3 Hydrochemical analyses

We analysed the AT concentration by performing a potentiometric titration using a Metrohm 888 Titrando with an Aquatrode pH probe. The recovery was ≥99%. We used a Marianda VINDTA 3C (Versatile Instrument for the Determination of Titration Alkalinity) to determine the DIC concentration by coulometric titration. The precision was ±2 μmol L^{-1} (Shadwick et al., 2011). AT and DIC measurements were calibrated against certified reference materials (CRMs) provided by Andrew Dickson (Scripps Institution of Oceanography). We calculated pH and pCO_2 by using the program CO2SYS (Pierrot et al., 2011), providing AT, DIC and water temperature, and using the freshwater equilibrium constants from Millero (1979). δ^{13}C-DIC were measured by means of continuous-flow isotope-ratio-monitoring mass spectrometry (CF-irmMS) using a Finnigan MAT 253 gas mass spectrometer coupled to a gas bench (GasBench II, Thermo Fisher Scientific) via a ConFlo IV continuous flow interface following the procedure described by Winde et al. (2014). Precision of δ^{13}C-DIC analysis was better than ±0.1‰. Results are given versus the VPDB standard. Stable water isotopes (δ^{18}O-H_2O and δ^2H-H_2O) were measured by means of cavity ring-down spectroscopy (CRDS) using a Picarro L2140-I system. International besides inhouse standards were used to scale the water isotope measurements (Böttcher and Schmiedinger, 2021). Stable isotope results are given in the conventional δ-notation versus the VSMOW standard and had a precision of better than ±0.06‰ for oxygen and ±0.3‰ for hydrogen isotopes (Böttcher and Schmiedinger, 2021). All stable isotope data given in '‰' are equivalent to 'mUr' (milli Urey; Brand and Coplen (2012)). Multielement composition (Al, Ba, Ca, Fe, K, Mg, Mn, Na, P, Si, Sr) was analysed by inductively coupled plasma optical emission spectrometry (ICP-OES) using a Perkin Elmer Optima 8300DV spectrometer. We determined anion concentrations (Br⁻, Cl⁻, F⁻, NO_3^-, SO_4^{2-}) using a Thermo Fisher Scientific Dionex ICS-2100 ion chromatograph. The precision for multielement and anion analyses was ±10%. The complete hydrochemical data set will beis available through PANGAEA at https://doi.org/10.1594/PANGAEA.952905.

2.4 Geospatial analyses

We delineated stream networks and watershed areas using the SAGA-GIS modules "Channel Network and Drainage Basins" and "Upslope Area" (Conrad et al., 2015) in QGIS 3.22.2 (QGIS.org, 2022) from the gridded digital elevation model
270 ArcticDEM (Porter et al., 2018) and used ArcGIS Pro 2.8.0 (ESRI, 2022) to create the maps. While we used the full resolution model (2 m) for the two small headwater catchments Gaskabohki and Guovzilbohki, we used the 32 m-resolution one for the larger watersheds.

We calculated the catchments' mean values of terrain roughness, permafrost probability, peatland cover, enhanced vegetation index (EVI) and bedrock lithology. We computed terrain roughness, which is indicative of the potential for physical erosion
275 (Riley et al., 1999), by using the GDAL tool "Roughness" (Rouault et al., 2022). We determined permafrost probability by using the Northern Hemisphere permafrost map based on TTOP (temperature at the top of the permafrost) modelling for 2000–2016 at 1 km^2 scale, which performs well in sparsely vegetated tundra regions and mountains (Obu et al., 2019), reflecting our study region. We determined the areal proportion of peatland cover, including mires, from the peatland map of Europe (Tanneberger et al., 2017). EVI can serve as a proxy for vegetation productivity (Huete et al., 2002). We used the EVI of the
280 MODIS vegetation index (VI) products, which is based on MODIS data with a resolution of 250 m from October 6th 2020 (Didan et al., 2015). We determined the lithological coverage of the smaller basins (Gaskabohki, Guovzilbohki and Bahkiljohka) from the Norwegian bedrock map "Berggrunn N250" (NGU, 2022) by calculating the area of the individual rock types (e.g., quartzite) as a percentage of the total catchment area. For the comparison with the larger catchments, we used the global lithological map database GLiM, which contains 16 lithological classes (Hartmann and Moosdorf, 2012).
285 We determined the riparian zone in the Gaskabohki catchment by first calculating the slope per 2 x 2 m DEM cell and then, starting from the streambed, identifying all cells belonging to the riparian zone that had a slope less than 10° (gradient of 1 : 5.7). We chose slope as the main criterion for defining the riparian zone because Camporese et al. (2014) found that the primary control on the nonlinear catchment response to a rainfall-runoff event is exerted by topography.

2.5 Modelling of soil respiration

290 We used the streamCO2-DEGAS model by Polsenaere and Abril (2012) to calculate initial soil pCO_2. The model first simulates the decrease in pCO_2 and increase in δ^{13}C-DIC that occur along the stream watercourse during degassing, starting from an assumed initial soil pCO_2 and ending at the in situ pCO_2 or δ^{13}C-DIC. Subsequently, soil pCO_2 is adjusted until pCO_2 and δ^{13}C-DIC simultaneously reach the in situ measured values. Soil organic matter isotopic composition and the isotopic fractionation of CO_2 in the soil due to selective molecular diffusion of the gas through the soil pores are considered. The model
295 is applicable for small, unproductive streams (assumption of insignificant primary production in the aquatic system) with acidic pH (4.6 – 7.2) and demands the input variables of AT, δ^{13}C-DIC, pCO_2, and stream temperature (Polsenaere and Abril, 2012). We assumed a proportion of non-carbon based acid induced alkalinity generation of 0.2 and a proportion of in-stream

respiration of 0. We also explored how alternative values for the proportion of non-carbon based acid induced alkalinity generation and in-stream respiration would affect the calculations of the initial soil pCO_2.

3 Results and discussion

3.1 Weathering and alkalinity generation in the Gaskabohki catchment

During the study period of fall 2020, the Gaskabohki catchment showed a mean AT concentration ($\pm$ standard deviation) of 125 ($\pm$ 5) µmol L^{-1} and a mean DIC concentration of 148 ($\pm$ 21) µmol L^{-1}. As the Gaskabohki catchment is mainly underlain by quartzite and arkose, thus the alkalinity-bearing mineral being feldspar, it is reasonable that the measured AT concentration exactly matches the concentration of 125 µmol L^{-1} that Meybeck (1987) found for catchments draining pure silicate bedrock, with more than 90% of the samples taken during non-flood periods. However, we would like to point out that the catchments studied by Meybeck (1987) are from temperate regions and ours are from Arctic regions.

3.1.1 Carbonic-acid induced carbonate weathering dominates alkalinity generation

The mean sum of major cation concentrations (Na$^+$, K$^+$, Ca^{2+}, Mg^{2+}) in the Gaskabohki stream was 120 ($\pm$ 4) µmol L^{-1}. This is consistent with the lower range found for rivers of the Canadian Shield in the Grenville Province (71-175 µmol L^{-1}) which are characterized by a similar catchment geology (Millot et al., 2002). The average Ca^{2+}/Na$^+$ and Mg^{2+}/Na$^+$ molar ratios in the Gaskabohki stream were 0.74 ($\pm$ 0.05) and 0.49 ($\pm$ 0.02), respectively. These values are consistent with the ones found by Meybeck (1986) for quartz sand and sandstone watersheds, and slightly higher than the ones calculated by Gaillardet et al. (1999) for the global silicate end-member. As we did not correct our data for precipitation due to the lack of rainwater composition data at the study site, these molar ratios are likely underestimated. Therefore, the weathering load would move closer to the carbonate end-member. In our data set, the highest Ca^{2+}/Na$^+$ molar ratios (up to 0.83) are associated with both the highest AT and the highest electrical conductivity values, indicating enhanced carbonate weathering. Considering that our ionic concentrations are not corrected for rainwater input, these elevated Ca^{2+}/Na$^+$ molar ratios, if corrected, should approach the molar ratio (Ca^{2+}/Na$^+$ > 1) reported by Oliva et al. (2004) for a weathering load that is extensively influenced by trace minerals such as calcite in high elevation systems draining granitic environments.

The DIC system of the Gaskabohki catchment is neither completely kinetically- (mineral weathering reactions) nor completely equilibrium- (mixing with atmospheric and biotic CO$_2$) controlled. It is controlled both by HCO$_3^-$ production from carbonate weathering and by the CO$_2$ pool in the soil (Fig. 2a). While the DIC system mainly consists of HCO$_3^-$ ions (~83 ($\pm$ 7) %), CO$_2^*$ plays a minor role (~16 ($\pm$ 9) %) and CO$_3^{2-}$ ions (~1 ($\pm$ 3) %) are negligible. We found that AT increases linearly with electric conductivity (adjusted R^2 = 0.81), suggesting that the Gaskabohki catchment is mainly controlled by mineral weathering (Fig. 2b). We excluded the measurement with the highest daily precipitation sum of 4.7 mm (4.3 mm within 3 h) from the linear regression (Fig. 2b, (i)), because this measurement showed a distinctly higher δ^{18}O-H$_2$O value when compared to the other measurements, thus indicating the highest proportion of surface water. Furthermore, this measurement also showed a

distinctly higher turbidity. As mineral weathering in headwater catchments is generally associated with groundwater inputs (Shin et al., 2011), we thought this exclusion reasonable. Other authors (Hill and Neal, 1997) explained decreases in AT associated with increases in electric conductivity with enhanced soil- and surface-derived components, such as nutrients and organic acids. We can also observe this in our data set, where we detected a nitrate signal in the samples which were taken during a day with rainfall or on up to four days that followed, before falling under the detection limit, indicating a hysteresis effect (Fig. 3).
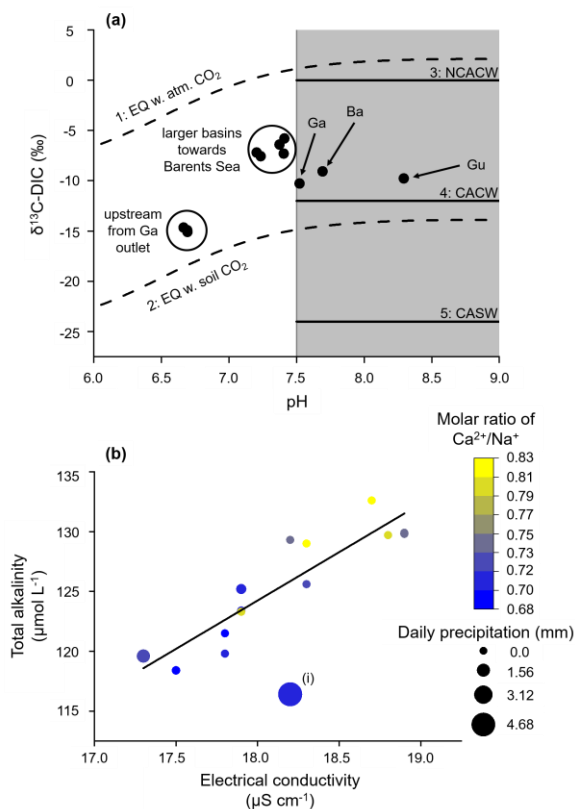
Figure 2: Equilibrium- vs. – kinetically-controlled systems. (a) If the pH of the stream water is below 7.5, then the DIC system is equilibrium-controlled, meaning that the stream DIC is in equilibrium with a large pool of either atmospheric (1) or soil (2) CO_2. The δ^{13}C-DIC values (dashed lines) were calculated based on the temperature-dependent fractionation factors that partition the carbon isotopes among

the DIC species (Zhang et al., 1995). If the pH is above 7.5, the DIC system is kinetically-controlled and three weathering pathways can be identified. Depending on the δ^{13}C-DIC value, the DIC originates from (3) NCACW (non-carbon based acid induced carbonate weathering), (4) CACW (carbonic acid induced carbonate weathering), (5) CASW (carbonic acid induced silicate weathering). Ga: Gaskabohki catchment; Gu: Guovzilbohki catchment; Ba: Bahkiljohka catchment. The figure was adjusted from Lehn et al. (2017). (b) AT as a function of electrical conductivity for the Gaskabohki catchment. The linear increase of AT with electrical conductivity indicates that mineral weathering is a major control in this catchment (y-intercept = -21.2 μmol L^{-1}, slope coefficient = 8.1). (i) We excluded this data point from the linear regression, as it shows the highest δ^{18}O-H$_2$O value, thus indicating the highest proportion of surface water.

We assumed the δ^{13}C-DIC endmember for carbonic acid induced carbonate weathering to be at about -12‰, as the vegetation at Iskorasfjellet is of C3 type characterized by a δ^{13}C value of about -27‰ (Kjellman et al., 2018). With the diffusive fractionation in low temperature waters, such as during fall in this subarctic region, causing a positive shift of about 3‰, the δ^{13}C value of the CO$_2$ pool would be about -24‰ (Deines et al., 1974; Michaelis et al., 1985; Zhang et al., 1995; Lehn et al., 2017). When dissolving carbonate minerals with a δ^{13}C value of about 0‰, the resulting δ^{13}C-DIC would thus be about -12‰. If the weathering agent is a non-carbon based acid, the δ^{13}C-DIC endmember for carbonate weathering will be about 0‰. As the mean δ^{13}C-DIC of the Gaskabohki catchment was -10.3 ($\pm$ 1.3) ‰, we attribute the alkalinity generation in the basin entirely to the dissolution of accessory carbonate rock by carbonic acid generated from soil respiration. We suggest that the small deviation from the carbonic acid induced carbonate weathering δ^{13}C-DIC endmember of -12‰ to slightly less negative values is caused by a small contribution from non-carbon based acid induced carbonate weathering. We believe, that the primary weathering agent of silicate minerals were non-carbon based acids, with no generation of DIC and AT.
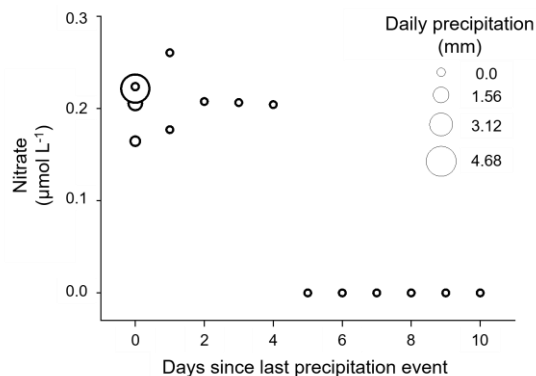
Figure 3: A nitrate signal is associated with a precipitation event and the days that follow. On the fifth day after the last precipitation event, we could not detect any more nitrate.

3.1.2 Carbonate weathering by sulphuric acid decreases alkalinity concentration

During the study period, AT was positively correlated with the concentration sum of Ca^{2+} and Mg^{2+} (adjusted $R^2 = 0.57$, Fig. 4a), which further confirms that alkalinity is produced from carbonate weathering alone. For one equivalent of a divalent cation, we found about two equivalents of alkalinity in our samples, as would be expected from carbonic acid induced carbonate weathering (see Eq. (1)). AT concentrations that fall below the regression line are associated with a high molar ratio of SO_4^{2-}/AT. We explain this with Ca^{2+} and Mg^{2+} originating from carbonate minerals that were dissolved by sulphuric acid. Thus, no AT, but SO_4^{2-} was generated. An indicator of the presence of sulphuric acid in the Gaskabohki catchment is that we observed a negative alkalinity concentration at a theoretical electrical conductivity of 0 (according to the linear regression in Fig. 2b, y-intercept $= -21.2$ μmol L^{-1}). We believe that sulphuric acid balances this negative alkalinity in the Gaskabohki catchment. In addition to sulphuric acid, organic acids could act as weathering agents for the carbonate minerals. Sulphuric acid could be generated from the oxidation of pyrite or reduced sulphur in wetlands, or be a remnant of acid ~~rain~~ raindeposition. Minor occurrences of pyrite are present in the upper parts of the Palaeoproterozoic bedrock of the Fennoscandian Shield (Sandström and Tullborg, 2009). As our study area is situated on the Karasjok Greenstone Belt, which forms the westernmost unit in a Palaeoproterozoic tectonic belt (Braathen and Davidsen, 2000), the generation of sulphuric acid by the oxidation of pyrite is a reasonable explanation. Another possibility for the generation of sulphuric acid could be the oxidation of reduced sulphur in wetlands (including permafrost) that accumulates during anoxic breakdown of organic matter. During dry periods or when permafrost thaws, reduced sulphur is oxidized to SO_4^{2-} and then typically released into drainage waters during the next flushing event. Even though acid rain deposition has decreased considerably since the end of the last century in northern Norway (Aas et al., 2021), the recovery from acid ~~rain~~ deposition in deeper soil horizons may be highly delayed (Berger et al., 2016; Marx et al., 2017b). This delayed soil acidification was also observed in southern Sweden, where the B2 horizon did not reach its most acidic conditions until 2013, almost 25 years after the sulphur deposition began to decline (McGivney et al., 2019). Our studied area could be influenced by legacy acid rain distributed area-wide from coal burning or, under the assumption of long-distance transport of pollutants, by the emissions of SO_2 from the smelters in Nikel and Zapoljarnij on the Kola Peninsula in Russia (linear distance between these two sites and Iskorasfjellet: ~200 km). A study in the Tibetian Plateau by Yuanrong et al. (2021) found that the sulphate concentration in glacial and permafrost streams was elevated compared to streams in other landscapes and explained this by condensed storage of acid deposition from long-distance transport during lower temperatures and a release during higher temperatures. Since the main wind directions on the Kola Peninsula in Russia are to the south and to the north (Chekushin et al., 1998) and the Russian smelters are located east of Iskorasfjellet, the sul~~ph~~furic acid could presumably originate from pyrite oxidation and legacy acid rain deposition from coal burning.

The δ^{13}C-DIC signal also reflects that two different weathering agents in the Gaskabohki catchment dissolve carbonate minerals. It shows a value of about -12‰ typical of carbonic acid induced carbonate weathering at a low molar ratio of SO_4^{2-}/AT (Fig. 4b). As the ratio increases, so does the δ^{13}C-DIC, suggesting an increased proportion of sulphuric acid as the weathering agent of carbonate minerals. We found that a logistic function better fit the data than a linear regression (adjusted

395 $R^2 = 0.78$ and 0.68, respectively), suggesting a change in weathering pathways. Therefore, regarding the CO_2 budget impacted by terrestrial weathering, the catchment can switch from a complete CO_2 sink to a partial CO_2 source. Since the $\delta^{13}C$-DIC depends on the molar ratio of SO_4^{2-}/AT and shows no correlation to discharge (Pearson correlation coefficient r = 0.02, not significant at $p < 0.01$), indicative of turbulence, we assume that the influence of CO_2 outgassing along the stream on the $\delta^{13}C$-DIC signal at the catchment outlet can be ignored.
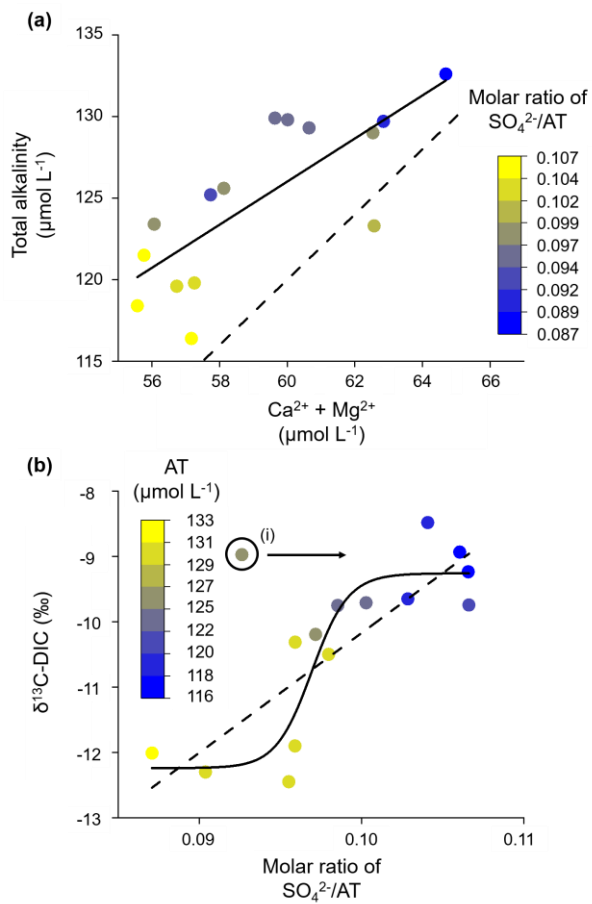
400

Figure 4: Alkalinity generation from carbonic acid induced carbonate weathering. (a) AT increases linearly with the concentration sum of Ca^{2+} and Mg^{2+}. At a constant concentration of divalent cations, AT decreases with increasing molar ratio of SO_4^{2-}/AT, indicating an increased proportion of carbonate weathering induced by sulphuric acid (release of divalent cations with no generation of alkalinity). Solid line: linear regression (y-intercept = 46.8 µmol L^{-1}, slope coefficient = 1.3); dashed line: representing the typical molar ratio of carbonic acid induced carbonate weathering of AT/(Ca^{2+} + Mg^{2+}) of 2:1. **(b)** δ^{13}C-DIC increases with the molar ratio of SO_4^{2-}/AT. The logistic fit (solid line) yielded a higher adjusted R^2 than the linear regression fit (dashed line: y-intercept = -28.5‰, slope coefficient = 183.3), suggesting that a changeover of weathering pathways explains the δ^{13}C-DIC signal better than a linear relationship. (i) We excluded this data point from both model fits, because it has a high pH, likely resulting from in-stream photosynthesis.

We excluded the point with the highest pH (pH = 9.6) from both data fits, which was characterized by a high δ^{13}C-DIC value and a low molar ratio of SO_4^{2-}/AT (see (i) in Fig. 4b), as it most likely experienced in-stream photosynthesis which would have lowered the SO_4^{2-}/AT molar ratio that was present when initially released into the stream. It is reasonable to assume photosynthesis, because we collected this sample during the afternoon on a day with a long sunshine duration, which would be ideal conditions for photosynthesis (Fig. 5). In addition, the Gaskabohki stream experiences no or only minimal canopy shading. Therefore, it is likely that in-stream photosynthesis during the course of the day consumed most of the CO_2 that was initially produced in the soil and released into the stream, increasing the pH and alkalinity.
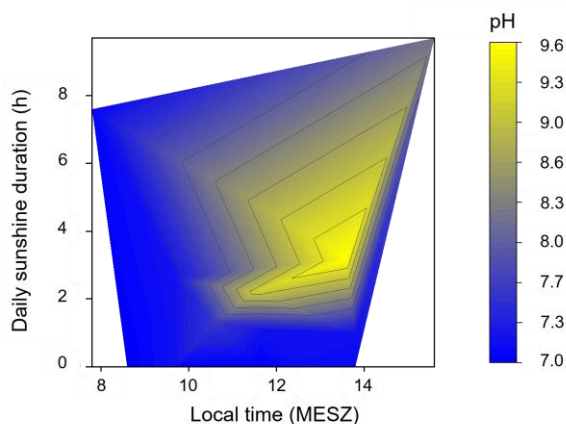
Figure 5: Heatmap showing the pH for different sampling times and sunshine durations. A high pH was measured in samples that were taken in the afternoon on a day with a high sunshine duration, indicating in-stream photosynthesis. The pH of samples that were collected in the morning were not affected by a high sunshine duration.

3.1.3 Carbonate-dominated riparian zone controls alkalinity signal

We propose that the AT signal is driven by preferential contribution from two different groundwater sources dominated by different weathering processes: (i) The first source is governed by carbonate minerals being dissolved almost exclusively by carbonic acid, which results in high AT concentrations and a low δ^{13}C-DIC value of about -12‰. (ii) The second source is governed by an increased proportion of sulphuric acid induced carbonate weathering in which no AT, but CO_2 and sulphate are produced and δ^{13}C-DIC is shifted to higher values of about -9‰ (Fig. 4b). Samples that show an intermediate δ^{13}C-DIC signal of about -11 to -9.5‰ represent a mixing of sources. We suggest that the first source (i) is situated in a wider riparian zone, ~1 km downstream of the spring and thus close to the catchment outlet, representing a hotspot of alkalinity release and the second source (ii) is stretched out upslope over the remainder of the catchment, representing ~99 % of the entire catchment area.

While almost the entire catchment is underlain by silicates with only accessory calcite from shale as the alkalinity-bearing lithology, the downstream riparian zone coincides with bedrock of partly calcareous quartz feldspar shale. Therefore, the downstream riparian zone that crosses this carbonate-enriched bedrock in the lower reaches of the watershed (Fig. 1d) bears a greater potential for carbonate weathering. In addition to its advantageous lithological properties, we propose that the downstream riparian zone, if ~~undisturbed~~not disturbed by a precipitation event, dominates the alkalinity concentration of the Gaskabohki catchment due to an enhanced hydrological connectivity. Increased soil moisture and hydrological flowpaths ~~shallower water tables near the stream~~ enable both the transport of weathering agent, in the form of soil respired CO_2, to the weatherable material and the transport of weathered products from the groundwater to the stream. That the weathering processes in the carbonate occurrences in the downstream riparian zone ~~is~~ are mainly responsible for the alkalinity signal is also reflected in Fig. 2a: While the samples of the three upstream sampling stations, which are characterized by a narrow riparian zone underlain by silicate minerals, are equilibrium-controlled and show a low mean HCO_3^- / CO_2 molar ratio of 1.3-1.4, the samples from the catchment outlet, which includes the larger downstream riparian zone crossing through the carbonated-enriched bedrock, are kinetically controlled and show a higher mean HCO_3^- / CO_2 molar ratio of 4.9, indicating enhanced alkalinity generation. Li et al. (2013) also recognized that in the dry season the land cover in the riparian zone much better explained the major elements in the river than the land cover over the entire catchment.

3.1.4 Precipitation event temporarily reduces control of the riparian zone

We found that a larger precipitation event on the fourth day of sampling caused a drastic decrease in AT at the outlet of the catchment, reducing AT to 116 μmol L^{-1}, the minimum value during our sampling campaign (Fig. 6a, 'day 0' corresponds to the day of the precipitation event). We explain this with a high proportion of surface water from precipitation which diluted the AT signal. This dilution effect can also be observed for the entire data set when plotting AT as a function of δ^2H-H_2O: AT generally decreased with increasing δ^2H-H_2O (Fig. 6b). When surface water mixes with the alkalinity-charged groundwater, the AT concentration measured in the stream is reduced.
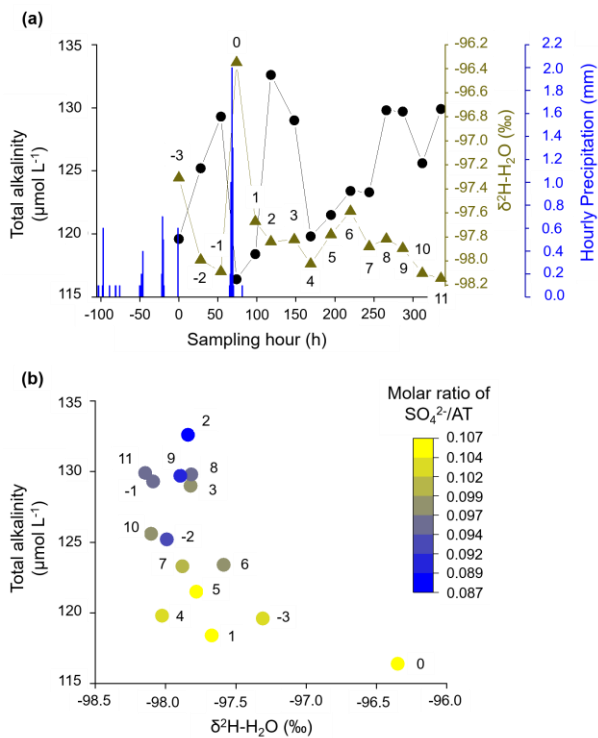
Figure 6: Alkalinity concentration is influenced by precipitation. (a) Variation of AT, δ^2H-H$_2$O and hourly precipitation over the course of the sampling campaign. **(b)** AT decreases with increasing δ^2H-H$_2$O, i.e., increasing contribution from surface water. At constant δ^2H-H$_2$O, AT decreases with increasing molar ratio of SO$_4^{2-}$/AT, indicating an increased contribution from the uphill catchment to the weathering load. Numbers next to data points show the number of days before (negative values) and after (positive values) the major rain event (0).

On the second day after the rain event ('day 2'), the AT concentration increased considerably up to 133 μmol L^{-1}, the maximum value in our time series. This coincided with a minimum molar ratio of SO$_4^{2-}$/AT, indicating that groundwater from the downstream riparian zone is maximally distributed to the stream water without being diluted by other sources. Petrone et al. (2007) also found that saturated riparian soils and precipitation mainly influence the storm chemistry for a low-permafrost watershed.

465 After a fast initial surface water response to the precipitation event ('days 0 and 1'), alkalinity-charged groundwater from the downstream riparian zone dominated the stream water signal ('days 2 and 3'). Consequently, we describe the catchment storage-discharge relationship as a clockwise loop with streamflow responding faster than groundwater. On the fourth day after the precipitation event ('day 4'), the AT concentration is reduced once more to 120 μmol L^{-1}. However, when compared to the last drop in the AT signal directly after the precipitation event ('day 0'), this decrease cannot be explained with dilution

470 from direct surface water, as the δ^2H-H_2O stayed on a low level. We rather attribute this decrease in AT to an increased contribution from uphill groundwater flow, which is dominated by an increased proportion of sulphuric acid-induced carbonate weathering, as the molar ratio of SO_4^{2-}/AT is high. The δ^2H-H_2O signal slightly increased again ('day 4 – 6'), indicating a delayed contribution from new water of the precipitation event. We suggest that some of the precipitation did not go directly to runoff, but infiltrated the soil of the uphill catchment, mixed with old water and created delayed runoff ('day 5 and 6').

475 Similarly, in a study about an Arctic watershed in northern Alaska, McNamara et al. (1997) reported that with ongoing thawing season, the storage capacity of the watershed increased, and in conjunction with this, that more new water entered the soil and mixed with old water, as opposed to going directly to runoff. Furthermore, this delayed contribution of uphill groundwater to the stream signal is related to generally larger time scales for subsurface processes. Myrabø (1997) and Camporese et al. (2014) found a similar hysteresis in the catchment storage-discharge relationship. For a riparian zone located in a deeply incised

480 glacial till valley in Indiana, USA, Vidon (2012) reported a quick rise of the water table near the stream and a concomitant decrease in hillslope water contributions to the stream during a storm event. In general, shallower water tables, which characterize riparian zones, frequently respond much more strongly to water infiltration than deeper water tables (Meyboom, 1967). Moreover, for most storms, Vidon (2012) observed the development of a water table down valley gradient. In our study, during the next days after the second decrease in AT ('days 5 – 8'), the AT signal slowly recovered, which coincided with a

485 decrease in the molar ratio of SO_4^{2-}/AT, i.e., a declining influence from the uphill catchment (Fig. 6b).

In conclusion, we identify the downstream riparian zone and the hillslope as two key catchment units that ~~collect and transfer water to the stream~~exchange water with the stream, as was shown by other authors before (McGlynn and Seibert, 2003; McGlynn and McDonnell, 2003b, 2003a). Usually, in headwater catchments, hillslopes are assumed to be the main contributor to streamflow (Seibert et al., 2009; McGuire and McDonnell, 2010; Vidon, 2012). In our data set, however, we observed that

490 the riparian zone responded more quickly to the precipitation event, probably due to higher antecedent soil moisture and a shallower groundwater table. The stable water isotope composition of all our stream water samples only slightly deviates from the regional and global meteoric water lines (Fig. 7), indicating that the groundwater contribution to stream water most likely originated from shallow groundwater. The average isotopic composition of local precipitation closely reflects the isotopic compositions of shallow groundwater (Fritz et al., 1987). The fall of 2020 was comparatively dry, which may have resulted in

495 particularly pronounced decoupling of uphill groundwater from the stream.
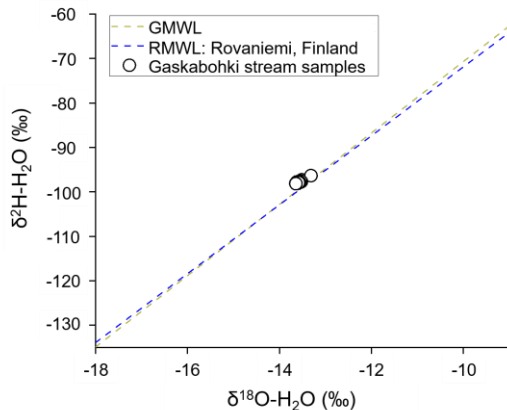
Figure 7: Stable water isotope composition. The stable water isotope compositions of the Gaskabohki stream water samples plot closely to the global (GMWL) and regional (RMWL) meteoric water line. RMWL line (y-intercept = 5.6‰, slope coefficient = 7.7) is based on monthly integrated samples collected between January 2004 and December 2019 at the GNIP (Global Network of Isotopes in Precipitation) station in Rovaniemi, Finland (International Atomic Energy Agency, 2020).

On the three days prior to the major precipitation event ('days -3 – -1'), AT showed an increasing trend, while δ^2H-H$_2$O was decreasing. Even though the rainfall intensity on the first day of sampling was not as high as on the fourth day, a contribution of surface water was evident in the δ^2H-H$_2$O signal. Therefore, AT was comparatively low at the beginning of sampling, which is due to a longer, albeit less intense, rain period on a few days prior to the first day of sampling, and thus dilution by surface water. This longer rain period most likely also activated the release of soil-stored nitrate into the stream, which lasted until the fourth day after the last day with rainfall (Fig. 3). This agrees with observations of Dingman (1971) over a small subarctic catchment with discontinuous permafrost in Alaska, where he found that streamflow recessions are dominated by a combination of through~~tunnel~~ flow under moss-covered parts of the basin and typical groundwater flow through the moss and soils.

3.1.5 Silicate weathering with minor alkalinity generation

Based on the δ^{13}C-DIC signal and the Na/(Ca^{2+} + Mg^{2+}) and SO$_4^{2-}$/AT molar ratios (see below), w~~W~~e suggest that the products from silicate weathering originate ~~are~~ to a large extent from sulphuric acid induced silicate weathering and are from groundwater of the uphill catchment upstream from the carbonate hotspot riparian zone. Accordingly, these products appear to have the same place of origin as~~released together with~~ the products ~~origination~~ from ~~carbonate~~ weathering of the accessory calcite minerals from shale, which are increasingly ~~by an increased~~ released by ~~proportion of~~ sulphuric acid induced weathering

from the uphill catchment. ~~from the groundwater of the catchment upstream from the carbonate hotspot riparian zone.~~ Except for this downstream riparian zone, the entire catchment is underlain by silicates with only accessory calcite from shale as the alkalinity-bearing lithology. Based on the δ^{13}C-DIC signal, silicate bedrock is dissolved by sulphuric acid alone, with no generation of DIC. However, some excess alkalinity remains when balancing AT with divalent cations (see dashed line in Fig. 4a, representing the typical molar ratio of carbonic acid induced carbonate weathering of AT/($Ca^{2+} + Mg^{2+}$) of 2:1). Therefore, we assume that silicate rocks are also weathered by carbonic acid to a small extent. However, when carbonic acid becomes available through soil respiration, it preferentially reacts with the accessory carbonate minerals due to faster dissolution kinetics. Weathering of silicate rocks in the Gaskabohki catchment contributes only minimally to CO_2 fixation. Interestingly, theoretical alkalinity production through carbonate weathering (dashed line) deviates most from actual production (solid line) at low concentration sums of Ca^{2+} and Mg^{2+} and high molar ratios of SO_4^{2-}/AT. These are the data points that we associate with increased groundwater contribution from the uphill catchment area, where silicate rock clearly dominates the composition of underlying bedrock over accessory carbonate from shales.

In the previous section (3.1.4), we used the molar ratio of SO_4^{2-}/AT as an indicator for the solute contribution from the uphill catchment to the stream water signal at the catchment outlet. This molar ratio is positively correlated with the molar ratio of Na/($Ca^{2+} + Mg^{2+}$) (adjusted $R^2 = 0.72$), indicating that SO_4^{2-}/AT can also be used as a tracer for solute contributions from uphill silicate weathering (Fig. 8a). When the silicate cationic load increases in relation to the carbonate cationic load (Na/($Ca^{2+} + Mg^{2+}$)), AT linearly decreases (adjusted $R^2 = 0.65$, Fig. 8b). As silicate bedrock is weathered by sulphuric acid, Na^+ and SO_4^{2-} are the main weathered products from silicate weathering in the groundwater in the uphill catchment, with no generation of AT.
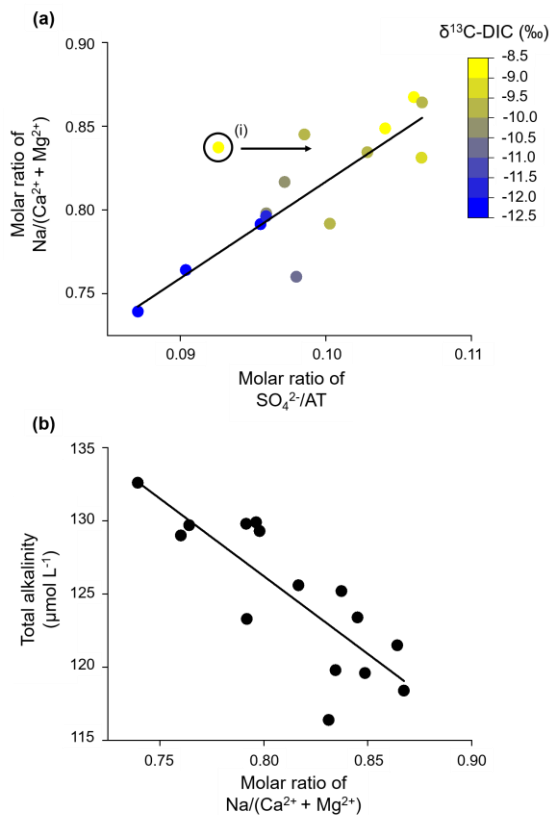
Figure 8: Uphill silicate weathering. (a) Molar ratio of $Na/(Ca^{2+} + Mg^{2+})$ increases linearly with the molar ratio of SO_4^{2-}/AT, indicating that the uphill silicate cation load behaves similar to the weathering load originating from sulphuric acid induced carbonate weathering. (i) We excluded this data point from the linear regression (y-intercept = 0.24, slope coefficient = 5.8), because it has a high pH, likely resulting from in-stream photosynthesis. **(b)** AT decreases linearly with the molar ratio of $Na/(Ca^{2+} + Mg^{2+})$, indicating that AT is only minimally released from the weathering of the abundant silicate bedrock. Instead, sulphuric acid acts as the main weathering agent; linear regression: y-intercept = 211.1 µmol L^{-1}, slope coefficient = -106.1.

3.1.4 Availability of weathering agent

545 The Gaskabohki stream was on average undersaturated with CO_2 (pCO_2 = 371 (± 219) ppm) with respect to atmospheric pCO_2, but reached a maximum pCO_2 of 651 ppm. By investigating a global compilation of streams and rivers, Marx et al. (2017a) found that catchments with areas up to 500 km^2 show consistently high maximum pCO_2 values of ~80,000 ppm. The maximum value we measured during the sampling period in fall 2020 was two orders of magnitude lower. This discrepancy can be explained by the fact that soil respiration in this subarctic region is generally lower compared to the global average, as annual

550 soil respiration decreases with latitude (Warner et al., 2019). Furthermore, with decreased temperatures in the fall, soil respiration was reduced when compared to the summer, during which soil respiration is highly elevated. In a study about CO_2 supersaturation in a temperate hardwood-forested catchment, soil pCO_2 was modelled between 907 ppm in winter and 35,313 ppm in summer (Jones and Mulholland, 1998). Another study about soil respiration in permafrost-affected tundra and boreal ecosystems in Alaska and Northwest Canada also recognized the summer time as the main driver of annual soil

555 respiration and calculated that summer months contributed to 58% of the regional soil respiration, winter months contributed to 15%, and the shoulder months contributed to 27% (Watts et al., 2021).

As the mean pH at the "Gaskabohki 1" sampling station, located ~700 m upstream from the outlet and ~400 m downstream of the spring, was 6.7 (± 0.0) and thus DIC was present in the form of CO_2^* from respiration of terrestrial organic matter and HCO_3^- from rock weathering, we were able to model the initial CO_2 released from soils to surface waters according to the

560 streamCO$_2$-DEGAS model by Polsenaere and Abril (2012). We then used this modelled upstream soil pCO_2 as a proxy for the entire Gaskabohki catchment, to which the streamCO$_2$-DEGAS model could not be applied, as the mean pH at the outlet was 7.5 (± 0.8), hence most of DIC was only in the form of HCO_3^-. With a mean modelled soil pCO_2 of 2009 (± 471) ppm during fall 2020, the Gaskabohki catchment is characterized by a rather low soil respiration signal when compared to a basin with similar catchment characteristics, but with an annual average temperature of 5.5 °C, situated in northern Czech Republic,

565 which showed a modelled soil pCO_2 of 1828-94,454 ppm during fall 2014 (Marx et al., 2018). Our mean modelled soil pCO_2 was likely lower due to lower temperatures and less rainfall. When the assumed value for the proportion of non-carbon based acid induced alkalinity generation is increased from 0.2 to 0.4, the modelled soil pCO_2 decreases by 13% to 1755 ppm. Thus, a moderate change in the assumed proportions of weathering agents results in a change in soil pCO_2 that is within one standard deviation. We consider an even higher value than 0.4 to be unrealistic, since we were able to show that the alkalinity was

570 generated from weathering by carbonic acid. A more pronounced effect on modelled soil pCO_2 occurs when the assumed proportion of in-stream respiration is increased: When the value is raised from 0.1 to 0.4, modelled soil pCO_2 increases by 52% to 3044 ppm. This value is no longer within one standard deviation of the original assumed conditions. Compared to the variations in soil pCO_2 determined by Marx et al. (2018) for the basin in the Czech Republic, the effect we found is small and soil pCO_2 remains at a comparatively low level.

575 These comparatively low values might explain why the abundant silicate bedrock is almost exclusively weathered by sulphuric acid instead of carbonic acid from soil respiration. When carbonic acid is available, it mainly reacts with the accessory

Formatiert: Tiefgestellt

Formatiert: Tiefgestellt

Formatiert: Tiefgestellt

Formatiert: Tiefgestellt

Formatiert: Tiefgestellt

Formatiert: Tiefgestellt

carbonate in the shale layers due to more favourable reaction conditions. We propose that only in the riparian zone along the channel, where soil moisture is highest, soil-respired CO_2 is efficiently transported down to the weathering zone.

When looking at individual pCO_2 values in the stream at the "Gaskabohki 1" sampling station, we recognized that a precipitation event caused the highest pCO_2 and when no rain fell, a higher temperature resulted in a higher pCO_2. We explain this finding with precipitation causing an increased connectivity of CO_2-rich soil solutions with the stream, comparable to the increased washout that we observed for soil-stored nitrate (Fig. 3), and higher temperatures causing increased soil respiration. We propose that the in situ weathering rates of carbonate minerals by carbonic acid are moderately activated in the fall due to relatively low CO_2 levels. We suggest that these rates are highest during the summer time, when soil respiration is most activated by elevated temperatures. During that time, groundwater concentrations of alkalinity from carbonic acid induced carbonate weathering should be highest. Therefore, we propose that the efficient hydrological flowpaths in the downstream riparian zone with facilitate its efficientthe transport of soil CO_2 to the weathering zone, and its shallow groundwater table is being mainly responsible for maintaining high AT concentrations in the Gaskabohki stream.

3.2 Controlling factors on alkalinity across watershed scales

No rain fell on the two days on which we extended the sampling to the further catchments up to the Tanafjord. In addition, no precipitation was detected up to seven days before. Thus, a dilution effect, which could be more pronounced in some catchments than others, did not need to be considered. Accordingly, we compared the alkalinity concentration without further normalization and an unconstrained investigation of the factors influencing alkalinity production should be granted.

3.2.1 Decreasing permafrost probability enhances hydrological connectivity

First, we will compare the three catchments, which are all situated on the mountainside of Iskorasfjellet: Gaskabohki, Bahkiljohka and Guovzilbohki. Compared to the Gaskabohki catchment, the Bahkiljohka catchment shows a higher stream water pH, therefore plotting further to the right in Fig. 2a, moving more to the site of the end-members for kinetically-controlled mineral weathering reactions. The Bahkiljohka catchment shows a larger catchment area and a lower permafrost probability than the Gaskabohki catchment (Tab. 1). Even more dominated by kinetically-controlled mineral weathering reactions, however, is the Guovzilbohki catchment. This watershed is a headwater catchment, like the Gaskabohki catchment. In contrast to the Gaskabohki catchment, whose bedrock area is only 0.5% partly calcareous quartz feldspar shale, however, about half (54%) of Guovzilbohki watershed is underlain by this carbonate-enriched bedrock. The Bahkiljohka catchment is characterized by an intermediate proportion (35%) of carbonate-containing lithology. Even though the areal carbonate extent in the Bahkiljohka catchment is not as high as in the Guovzilbohki catchment, it shows the highest AT concentration of 586 µmol L^{-1} (Fig. 9a). We assume that if a certain level of carbonate-containing lithology is present in the catchment, catchment area and permafrost probability control alkalinity generation. This is evident when AT measured in all the catchments studied is plotted as a function of permafrost probability (Fig. 9b). AT linearly decreases with permafrost probability (adjusted $R^2 = 0.28$). Decreases in HCO_3^- flux with increasing permafrost probability was also observed by Tank et al. (2012) for catchment across

the circumboreal realm. While permafrost probability, lithology and catchment area are first- and second-order controlling

610 factor on alkalinity concentration, terrain roughness, EVI and peat cover seem to play a subordinate role in our data set. However, we found that AT generally decreases with increasing terrain roughness and decreasing peat cover, with the Bahkiljohka catchment being an outlier in both correlations. Finally, we recognized a high degree of multicollinearity between permafrost probability and EVI (adjusted R^2 when plotting EVI as a function of permafrost probability = 0.63).

615

Table 1: Various catchment properties of the sampled streams and rivers. [1]mt: metamorphics ("wide variety of rocks from shales to gneiss, from amphibolite to quartzite"), [2]vb: basalt-type rocks, [3]pa: plutonic rocks containing quartz, [4]sm: mixed sedimentary rocks ("carbonate is mentioned but not dominant"), [5]sc: carbonate sedimentary rocks (Hartmann and Moosdorf, 2012).

	Catchment area (km^2)	Stream length (km)	Roughness	Permafrost probability	Areal proportion of peatland	EVI	Areal proportion of main lithology classes				
							mt[1]	vb[2]	pa[3]	sm[4]	sc[5]
Gaskabohki 1	0.2	0.4	25.5	0.13	0.00	0.29	1.00	0.00	0.00	0.00	0.0
Gaskabohki 2	0.2	0.6	25.8	0.13	0.00	0.29	1.00	0.00	0.00	0.00	0.0
Gaskabohki 3	0.4	0.8	27.8	0.13	0.00	0.28	1.00	0.00	0.00	0.00	0.0
Gaskabohki 4 (outlet)	0.7	1.1	27.7	0.13	0.00	0.28	1.00	0.00	0.00	0.00	0.0
Guovzilbohki	2.8	3.6	25.3	0.10	0.00	0.30	1.00	0.00	0.00	0.00	0.0
Bahkiljohka	78	20	19.8	0.04	0.06	0.30	0.76	0.16	0.00	0.06	0.0
Karasjohka 1	4909	162	11.5	0.17	0.16	0.27	0.69	0.10	0.08	0.11	0.0
Karasjohka 2	7255	187	12.9	0.14	0.18	0.28	0.67	0.16	0.06	0.08	0.0
Karasjohka 3	11614	297	15.9	0.14	0.15	0.27	0.76	0.11	0.04	0.06	0.4
Tanaelva 1	14085	357	15.8	0.13	0.15	0.27	0.69	0.11	0.10	0.07	0.5
Tanaelva 2	15156	384	15.9	0.13	0.14	0.28	0.65	0.10	0.10	0.12	0.3

620 As discussed in section 3.1 in detail for the Gaskabohki catchment, it seems that alkalinity generation is limited by the contact of weathering agent (CO_2 from soil respiration) with weatherable material as well as the transport of the weathered products out of the weathering zone into the stream. In the Gaskabohki catchment, the saturated riparian zone facilitates this hydrological transport. In the Bahkiljohka catchment, which shows the highest AT concentration, the low permafrost probability is most likely responsible for enhanced hydrological connectivity. In another study about the effects of permafrost loss on discharge

625 from a wetland-dominated, discontinuous permafrost basin, Stone et al. (2019) reported that total annual discharge from the channel fen decreased by 2.5 % for every 10 % decrease in permafrost area due to increased surface storage capacity, reduced run-off efficiency, and increased landscape evapotranspiration.
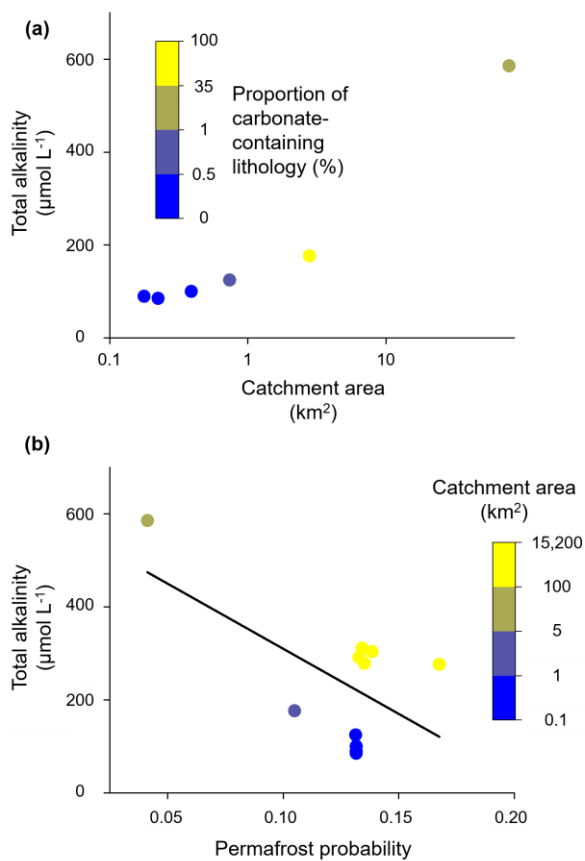
Figure 9: Controlling factors on alkalinity concentration across watershed scales. (a) At Iskorasfjellet, AT increases with catchment area and the proportion of carbonate-containing lithology. **(b)** At a larger spatial scale, AT is controlled by permafrost probability, with a low permafrost probability being associated with a high AT concentration. At a similar permafrost probability, a larger catchment area yields a higher AT concentration; linear regression: y-intercept = 590.0 μmol L^{-1}, slope coefficient = -2800.6.

At constant permafrost probability and thus similar hydrological conditions, AT increases with catchment area. From the in-depth study of the Gaskabohki catchment, we found that a precipitation event resulted in the highest turbidity values which we

associate with increased sediment supply to the stream. Therefore, intense precipitation events have the potential to activate the fluvial transport of suspended sediment supply ~~mineral substrate~~ downstream. This new material together with the surface water most likely leave the headwaters quickly. In the larger rivers downstream, however, this material can undergo several weathering cycles, increasing alkalinity. From decade-long hydrometeorological and biogeochemical observations of catchments in the High Arctic, Beel et al. (2021) deduced that increased late summer rainfall enhanced terrestrial-aquatic connectivity for dissolved and particulate material fluxes. Zolkos et al. (2020) showed that this particulate material, in their study on retrogressive thaw slumps, can rapidly weather during fluvial transport within runoff.

The DIC systems of the three small subcatchments situated within the Gaskabohki headwater catchment and the five larger catchments that drain into the Barents Sea are equilibrium-controlled (Fig. 2a). However, while the DIC species of the three small catchments mix with biotic CO_2, the DIC species of the five larger basins are rather in exchange with atmospheric CO_2. For undisturbed headwater catchments on the Peel Plateau in Canada, Zolkos et al. (2020) also reported that stream chemistry reflected CO_2 from soil respiration processes.

3.2.2 Alkalinity generation from carbonate weathering – from Iskorasfjellet to the Tanafjord

As we found in section 3.1.2 for the Gaskabohki catchment on the temporal scale, AT also linearly increases on the spatial scale with the concentration sum of Ca^{2+} and Mg^{2+} (adjusted R^2 = 0.98, Fig. 10a). Therefore, we propose that alkalinity is produced from carbonate weathering by carbonic acid in all basins that we studied – from Iskorasfjellet to the Tanafjord. While the Gaskabohki and Guovzilbohki headwater catchments with the two smallest concentration sums of Ca^{2+} and Mg^{2+} show the characteristic molar ratio of $AT/(Ca^{2+} + Mg^{2+})$ of 2:1, indicative for carbonate weathering by carbonic acid (see dashed line in Fig. 10a), the larger catchments show a reduced molar ratio. This decrease coincides with an increase in the molar ratio of SO_4^{2-}/AT, suggesting that the carbonate minerals are increasingly dissolved by sulphuric acid. In addition to the Gaskabohki catchment, sulphuric acid appears to be present in the other basins, because at a theoretical electrical conductivity of 0, the linear regression of AT as a function of electrical conductivity suggests a negative alkalinity (y-intercept = -16.9 μmol L^{-1}, adjusted R^2 = 0.99, Fig. 10b). Therefore, we assume that some of the divalent cations originate from sulphuric acid induced carbonate weathering, with no generation of AT, but CO_2 and SO_4^{2-}. Thus, carbonate weathering in the studied region does not only consume CO_2, but also releases CO_2, albeit to a lesser extent. Carbonic acid induced silicate weathering does not appear to contribute to alkalinity generation and thus to CO_2 sequestration (Fig. 2a), although silicate bedrock is generally more abundant in the study area than carbonate bedrock according to lithological maps (Tab. 1).
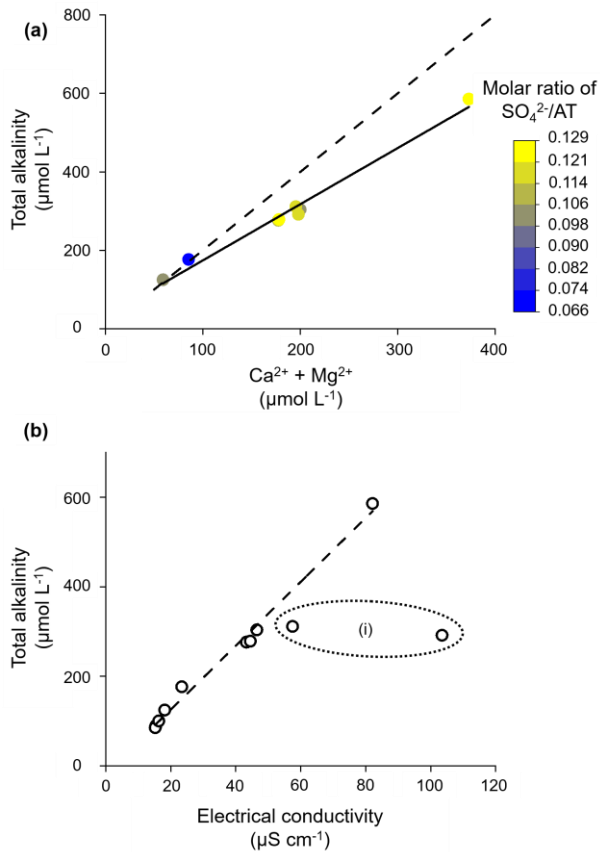
Figure 10: Alkalinity generation from carbonate weathering across watershed scales. (a) AT increases linearly with the concentration sum of Ca^{2+} and Mg^{2+}. Solid line: linear regression (y-intercept = 31.1 µmol L^{-1}, slope coefficient = 1.4); dashed line: representing the typical molar ratio of carbonic acid induced carbonate weathering of AT/(Ca^{2+} + Mg^{2+}) of 2:1. **(b)** AT increases linearly with electrical conductivity. (i) Dotted ellipse: We excluded these two data points from the linear regression (dashed line: y-intercept = -19.9 µmol L^{-1}, slope coefficient = 7.1), as they are characterized by distinctly higher Na^+ and Cl^- concentrations (https://doi.org/10.1594/PANGAEA.952905), indicating an influence from the salty fjord and seawater close by.

4 Conclusions

In the present study is shown that weathering of accessory carbonate dominates the alkalinity generation in a mainly silicate-dominated subarctic headwater catchment in Northern Norway. The vast Fennoscandian Shield is generally underlain by silicates as the alkalinity-bearing rock type. An area of ~20,000 km^2 of the Fennoscandian Shield, however, is classified as
675   metamorphic rocks with minor carbonate occurrences (Hartmann and Moosdorf, 2012), the same geology that dominates the Gaskabohki catchment. When transferring our results about the Gaskabohki catchment to the Fennoscandian Shield, we propose that alkalinity dynamics in this area are also drastically influenced by carbonate minerals, even though their occurrence may be low. Further, we have found that alkalinity generation by carbonate weathering greatly decreases when the proportion of sulphuric acid as the weathering agent increases. This was particularly evident in the larger catchments towards the
680   Tanafjord.

For the Gaskabohki headwater catchment, we identified the weathering processes in the carbonate-enriched bedrock located in the lower reaches of the catchment downstream riparian zone characterized by a carbonate-enriched lithology, as the main contributor to alkalinity in the stream. The efficient hydrological flowpaths in this areaThis riparian zone appears to facilitate both the transport of soil-respired CO_2 to the weathering zone und the transport of weathered products to the channel. When
685   undisturbed, high alkalinity concentrations (~130 μmol L^{-1}) are maintained by the inflow of alkalinity-charged groundwater from the downstream hyporheic riparian zone. However, after a precipitation event, the alkalinity concentration in the stream was reduced twice due to dilution: 1) immediately after the rain event, alkalinity was diluted by new surface water, and 2) after 4 to 7 days after the rain event, the signal was diluted again by a delayed contribution of uphill groundwater to the stream that contained reduced amounts of alkalinity.

690   Weathering of silicate rocks by carbonic acid, and hence long-term CO_2 sequestration, seems to be limited by insufficient contact between the weathering agent (CO_2^*) and the mineral surface. We expect silicate weathering rates to increase in the Gaskabohki headwater catchment due to climate change in the future, as both the permafrost extent is declining and the annual precipitation is increasing. These two trends will increase the water storage capacity, thereby increasing the contact time of weathering agent and weatherable material. McNamara et al. (1997) suggested that as the thickness of the active layer in
695   permafrost increases, not only will the hydrologic response of streams to precipitation inputs be attenuated due to greater water storage capacity, but also root and heterotrophic respiration will increase as it occurs almost exclusively in this thawed layer. Therefore, we expect the availability of weathering agent in the form of carbonic acid to increase.

In conclusion, we expect an increase in alkalinity generation from carbonic acid induced silicate weathering in the Gaskabohki catchment in the future, although we believe the feedback to be slow, as silicate weathering rates are several orders of
700   magnitude slower than carbonate weathering rates. We also propose that carbonic acid induced carbonate weathering is likely to increase. We suppose that alkalinity generation from carbonate weathering is responding faster to a changing climate. We believe that parts of the Fennoscandian Shield will experience a rapid weathering response of accessory carbonate minerals to

climate change in the future, resulting in elevated alkalinity levels. Future long-term studies that include more seasons and groundwater sampling are required to confirm this hypothesis.

705 *Data availability*. All data used in this study is available ~~through~~at PANGAEA ~~(*PANGAEA DOI Link*)~~at https://doi.org/10.1594/PANGAEA.952905.

Author contributions. NL, HL and HT designed the study. NL led the field research, coordinated laboratory analyses, and wrote the first draft of the manuscript. NL measured DIC concentration. AE measured cation and anion concentrations. MEB
710 and JH contributed (isotope) analytical measurements and data interpretation. All authors contributed to manuscript writing and editing.

Competing interests. The authors declare that the research was conducted in the absence of any commercial or financial relationships that could be construed as a potential conflict of interest.
715

Acknowledgements. We thank the German Federal Ministry of Education and Research (BMBF) for providing the funding for this project. NL and HT were supported by "The Ocean's Alkalinity: Connecting geological and metabolic processes and time-scales", BMBF under "Make our Planet Great Again – German Research Initiative", grant number 57429828, implemented by the German Academic Exchange Service (DAAD). We thank M. Treblin and L. Detjen for assistance in the field. JH wishes
720 to thank P. Bartsch for measuring AT concentration.

5 References

Aas, W., Eckhardt, S., Fiebig, M., Solberg, S., Platt, S. M., Yttri, K. E., and Zwaaftink, C. G.: Monitoring of long-range transported air pollutants in Norway: NILU report 13/2021, Norwegian Environment Agency, Kjeller, 2021.

725 Amiotte Suchet, P., Probst, J.-L., and Ludwig, W.: Worldwide distribution of continental rock lithology: Implications for the atmospheric/soil CO 2 uptake by continental weathering and alkalinity river transport to the oceans, Global Biogeochem. Cycles, 17, n/a-n/a, doi:10.1029/2002GB001891, 2003.

Amundson, R., Stern, L., Baisden, T., and Wang, Y.: The isotopic composition of soil and soil-respired CO2, Geoderma, 82, 83–114, doi:10.1016/S0016-7061(97)00098-0, 1998.

730 Appelo, C., Verweij, E., and Schäfer, H.: A hydrogeochemical transport model for an oxidation experiment with pyrite/calcite/exchangers/organic matter containing sand, Applied Geochemistry, 13, 257–268, doi:10.1016/S0883-2927(97)00070-X, 1998.

Beel, C. R., Heslop, J. K., Orwin, J. F., Pope, M. A., Schevers, A. J., Hung, J. K. Y., Lafrenière, M. J., and Lamoureux, S. F.: Emerging dominance of summer rainfall driving High Arctic terrestrial-aquatic connectivity, Nature communications, 735 12, 1448, doi:10.1038/s41467-021-21759-3, 2021.

Berger, T. W., Türtscher, S., Berger, P., and Lindebner, L.: A slight recovery of soils from Acid Rain over the last three decades is not reflected in the macro nutrition of beech (Fagus sylvatica) at 97 forest stands of the Vienna Woods, Environmental pollution (Barking, Essex 1987), 216, 624–635, doi:10.1016/j.envpol.2016.06.024, 2016.

Berner, E. K. and Berner, R. A.: The global water cycle: Geochemistry and environment, Prentice-Hall, Inc, Englewood 740 Cliffs, 397 pp., 1987.

Berner, R. A., Lasaga, A. C., and Garrels, R. M.: The carbonate-silicate geochemical cycle and its effect on atmospheric carbon dioxide over the past 100 million years, American Journal of Science, 283, 641–683, doi:10.2475/ajs.283.7.641, 1983.

Blum, J. D., Gazis, C. A., Jacobson, A. D., and Page Chamberlain, C.: Carbonate versus silicate weathering in the Raikhot 745 watershed within the High Himalayan Crystalline Series, Geol, 26, 411, doi:10.1130/0091-7613(1998)026%3C0411:CVSWIT%3E2.3.CO;2, 1998.

Böttcher, M. E.: The Stable Isotopic Geochemistry of the Sulfur and Carbon Cycles in a Modern Karst Environment, Isotopes in environmental and health studies, 35, 39–61, doi:10.1080/10256019908234078, 1999.

Böttcher, M. E. and Schmiedinger, I.: The impact of temperature on the water isotope (2H/1H, 17O/16O, 18O/16O) 750 fractionation upon transport through a low-density polyethylene membrane, Isotopes in environmental and health studies, 57, 183–192, doi:10.1080/10256016.2020.1845668, 2021.

Braathen, A. and Davidsen, B.: Structure and stratigraphy of the Palaeoproterozoic Karasjok Greenstone Belt, north Norway - regional implications, Norsk Geologisk Tidsskrift, 80, 33–50, doi:10.1080/002919600750042663, 2000.

Brand, W. A. and Coplen, T. B.: Stable isotope deltas: tiny, yet robust signatures in nature, Isotopes in environmental and 755 health studies, 48, 393–409, doi:10.1080/10256016.2012.666977, 2012.

Campeau, A., Wallin, M. B., Giesler, R., Löfgren, S., Mörth, C.-M., Schiff, S., Venkiteswaran, J. J., and Bishop, K.: Multiple sources and sinks of dissolved inorganic carbon across Swedish streams, refocusing the lens of stable C isotopes, Scientific reports, 7, 9158, doi:10.1038/s41598-017-09049-9, 2017.

760 Camporese, M., Penna, D., Borga, M., and Paniconi, C.: A field and modeling study of nonlinear storage-discharge dynamics for an Alpine headwater catchment, Water Resour. Res., 50, 806–822, doi:10.1002/2013WR013604, 2014.

Cerling, T. E., Solomon, D., Quade, J., and Bowman, J. R.: On the isotopic composition of carbon in soil carbon dioxide, Geochimica et Cosmochimica Acta, 55, 3403–3405, doi:10.1016/0016-7037(91)90498-T, 1991.

Chekushin, V. A., Bogatyrev, I. V., Caritat, P. de, Niskavaara, H., and Reimann, C.: Annual atmospheric deposition of 16 elements in eight catchments of the central Barents region, Science of The Total Environment, 220, 95–114,
765 doi:10.1016/S0048-9697(98)00247-2, 1998.

Conrad, O., Bechtel, B., Bock, M., Dietrich, H., Fischer, E., Gerlitz, L., Wehberg, J., Wichmann, V., and Böhner, J.: System for Automated Geoscientific Analyses (SAGA) v. 2.1.4, Geosci. Model Dev., 8, 1991–2007, doi:10.5194/gmd-8-1991-2015, 2015.

Davidson, G. R.: The stable isotopic composition and measurement of carbon in soil CO2, Geochimica et Cosmochimica
770 Acta, 59, 2485–2489, doi:10.1016/0016-7037(95)00143-3, 1995.

Deines, P., Langmuir, D., and Harmon, R. S.: Stable carbon isotope ratios and the existence of a gas phase in the evolution of carbonate ground waters, Geochimica et Cosmochimica Acta, 38, 1147–1164, doi:10.1016/0016-7037(74)90010-6, 1974.

Didan, K., Munoz, A. B., Solano, R., and Huete, A.: MOD13Q1 v006: MODIS/Terra Vegetation Indices 16-Day L3 Global
775 250 m SIN Grid, Land Processes Distributed Active Archive Center (LP DAAC), https://lpdaac.usgs.gov/, 2015.

Dingman, S. L.: Hydrology of the Glenn Creek watershed, Tanana River Basin, central Alaska: Res. Rep. 297, Cold Regions Research and Engineering Laboratory, Hanover, New Hampshire, USA, 1971.

Drake, T. W., Tank, S. E., Zhulidov, A. V., Holmes, R. M., Gurtovaya, T., and Spencer, R. G. M.: Increasing Alkalinity Export from Large Russian Arctic Rivers, Environmental science & technology, 52, 8302–8308,
780 doi:10.1021/acs.est.8b01051, 2018.

ESRI: ArcGIS pro, ESRI, Redlands, USA, 2022.

Frey, K. E. and McClelland, J. W.: Impacts of permafrost degradation on arctic river biogeochemistry, Hydrol. Process., 23, 169–182, doi:10.1002/hyp.7196, 2009.

Fritz, P., Drimmie, R. J., Frape, S. K., and O'Shea, K.: The isotopic composition of precipitation and groundwater in Canada,
785 IAEA, International Atomic Energy Agency (IAEA), 1987.

Gaillardet, J., Dupré, B., Louvat, P., and Allègre, C. J.: Global silicate weathering and CO2 consumption rates deduced from the chemistry of large rivers, Chemical Geology, 159, 3–30, doi:10.1016/S0009-2541(99)00031-5, 1999.

Garrels, R. M. and Berner, R. A.: The Global Carbonate-Silicate Sedimentary System — Some Feedback Relations, in: Biomineralization and Biological Metal Accumulation, Westbroek, P., Jong, E. W. de (Eds.), Springer Netherlands, Dordrecht, 73–87, 1983.

Gislason, S. R., Oelkers, E. H., Eiriksdottir, E. S., Kardjilov, M. I., Gisladottir, G., Sigfusson, B., Snorrason, A., Elefsen, S., Hardardottir, J., Torssander, P., and Oskarsson, N.: Direct evidence of the feedback between climate and weathering, Earth and Planetary Science Letters, 277, 213–222, doi:10.1016/j.epsl.2008.10.018, 2009.

Goll, D. S., Moosdorf, N., Hartmann, J., and Brovkin, V.: Climate-driven changes in chemical weathering and associated phosphorus release since 1850: Implications for the land carbon balance, Geophys. Res. Lett., 41, 3553–3558, doi:10.1002/2014GL059471, 2014.

Hartmann, J.: Bicarbonate-fluxes and CO2-consumption by chemical weathering on the Japanese Archipelago — Application of a multi-lithological model framework, Chemical Geology, 265, 237–271, doi:10.1016/j.chemgeo.2009.03.024, 2009.

Hartmann, J., Jansen, N., Dürr, H. H., Kempe, S., and Köhler, P.: Global CO2-consumption by chemical weathering: What is the contribution of highly active weathering regions?, Global and Planetary Change, 69, 185–194, doi:10.1016/j.gloplacha.2009.07.007, 2009.

Hartmann, J. and Moosdorf, N.: The new global lithological map database GLiM: A representation of rock properties at the Earth surface, Geochem. Geophys. Geosyst., 13, 119, doi:10.1029/2012GC004370, 2012.

Hill, T. and Neal, C.: Spatial and temporal variation in pH, alkalinity and conductivity in surface runoff and groundwater for the Upper River Severn catchment, Hydrol. Earth Syst. Sci., 1, 697–715, doi:10.5194/hess-1-697-1997, 1997.

Hoefs, J.: Contribution to the isotopic geochemistry of carbon in magmatic rocks, Goettingen Univ., Goettingen, Ger, Germany, 1973.

Huete, A., Didan, K., Miura, T., Rodriguez, E., Gao, X., and Ferreira, L.: Overview of the radiometric and biophysical performance of the MODIS vegetation indices, Remote Sensing of Environment, 83, 195–213, doi:10.1016/S0034-4257(02)00096-2, 2002.

International Atomic Energy Agency: Global Network of Isotopes in Precipitation. The GNIP Database, https://nucleus.iaea.org/wiser, 2020.

Jacobson, A. D., Blum, J. D., Chamberlain, C., Craw, D., and Koons, P. O.: Climatic and tectonic controls on chemical weathering in the New Zealand Southern Alps, Geochimica et Cosmochimica Acta, 67, 29–46, doi:10.1016/S0016-7037(02)01053-0, 2003.

Jacobson, A. D., Blum, J. D., Chamberlain, C., Poage, M. A., and Sloan, V. F.: Ca/Sr and Sr isotope systematics of a Himalayan glacial chronosequence: Carbonate versus silicate weathering rates as a function of landscape surface age, Geochimica et Cosmochimica Acta, 66, 13–27, doi:10.1016/S0016-7037(01)00755-4, 2002.

Jacobson, A. D., Grace Andrews, M., Lehn, G. O., and Holmden, C.: Silicate versus carbonate weathering in Iceland: New insights from Ca isotopes, Earth and Planetary Science Letters, 416, 132–142, doi:10.1016/j.epsl.2015.01.030, 2015.

Jones, J. B. and Mulholland, P. J.: Influence of drainage basin topography and elevation on carbon dioxide and methane supersaturation of stream water, Biogeochemistry, 40, 57–72, doi:10.1023/A:1005914121280, 1998.

Kempe, S.: Long-term records of CO_2 pressure fluctuations in fresh waters, Mitt. Geol.-Paläont. Inst. Univ. Hamburg;
825   SCOPE/UNEP Sonderband, 52, 91–332, 1982.

Kjellman, S. E., Axelsson, P. E., Etzelmüller, B., Westermann, S., and Sannel, A. B. K.: Holocene development of subarctic permafrost peatlands in Finnmark, northern Norway, The Holocene, 28, 1855–1869, doi:10.1177/0959683618798126, 2018.

Lag, J.: Soil Map Norway - Jordbunnskart, Norges Landbrukshogskole, https://esdac.jrc.ec.eu-1396 ropa.eu/content/soil-
830   map-norway-jord-bunnskart, 1983.

Land, L. S.: The isotopic and trace element geochemistry of dolomite: the state of the art, in: Concepts and Models of Dolomitization, Zenger, D. H., Dunham, J. B., Ethington, R. L. (Eds.), SEPM (Society for Sedimentary Geology), 87–110, 1980.

Lasaga, A. C.: Chemical kinetics of water-rock interactions, J. Geophys. Res., 89, 4009–4025,
835   doi:10.1029/JB089iB06p04009, 1984.

Lehn, G. O., Jacobson, A. D., Douglas, T. A., McClelland, J. W., Barker, A. J., and Khosh, M. S.: Constraining seasonal active layer dynamics and chemical weathering reactions occurring in North Slope Alaskan watersheds with major ion and isotope ($\delta 34SSO4$, $\delta 13CDIC$, $87Sr/86Sr$, $\delta 44/40Ca$, and $\delta 44/42Ca$) measurements, Geochimica et Cosmochimica Acta, 217, 399–420, doi:10.1016/j.gca.2017.07.042, 2017.

840 Li, S., Xia, X., Tan, X., and Zhang, Q.: Effects of catchment and riparian landscape setting on water chemistry and seasonal evolution of water quality in the upper Han River basin, China, PloS one, 8, e53163, doi:10.1371/journal.pone.0053163, 2013.

Li, S.-L., Calmels, D., Han, G., Gaillardet, J., and Liu, C.-Q.: Sulfuric acid as an agent of carbonate weathering constrained by $\delta 13CDIC$: Examples from Southwest China, Earth and Planetary Science Letters, 270, 189–199,
845   doi:10.1016/j.epsl.2008.02.039, 2008.

Li, S.-L., Liu, C.-Q., Li, J., Lang, Y.-C., Ding, H., and Li, L.: Geochemistry of dissolved inorganic carbon and carbonate weathering in a small typical karstic catchment of Southwest China: Isotopic and chemical constraints, Chemical Geology, 277, 301–309, doi:10.1016/j.chemgeo.2010.08.013, 2010.

Liu, J. and Han, G.: Effects of chemical weathering and CO_2 outgassing on $\delta 13CDIC$ signals in a karst watershed, Journal of
850   Hydrology, 589, 125192, doi:10.1016/j.jhydrol.2020.125192, 2020.

Liu, Z., Macpherson, G. L., Groves, C., Martin, J. B., Yuan, D., and Zeng, S.: Large and active CO_2 uptake by coupled carbonate weathering, Earth-Science Reviews, 182, 42–49, doi:10.1016/j.earscirev.2018.05.007, 2018.

Macpherson, G. L., Sullivan, P. L., Stotler, R. L., Norwood, B. S., Chudaev, O., Kharaka, Y., Harmon, R., Millot, R., and Shouakar-Stash, O.: Increasing groundwater CO_2 in a mid-continent tallgrass prairie: Controlling factors, E3S Web
855   Conf., 98, 6008, doi:10.1051/e3sconf/20199806008, 2019.

Marx, A., Conrad, M., Aizinger, V., Prechtel, A., van Geldern, R., and Barth, J. A. C.: Groundwater data improve modelling of headwater stream CO_2 outgassing with a stable DIC isotope approach, Biogeosciences, 15, 3093–3106, doi:10.5194/bg-15-3093-2018, 2018.

860 Marx, A., Dusek, J., Jankovec, J., Sanda, M., Vogel, T., van Geldern, R., Hartmann, J., and Barth, J. A. C.: A review of CO 2 and associated carbon dynamics in headwater streams: A global perspective, Rev. Geophys., 55, 560–585, doi:10.1002/2016RG000547, 2017a.

Marx, A., Hintze, S., Sanda, M., Jankovec, J., Oulehle, F., Dusek, J., Vitvar, T., Vogel, T., van Geldern, R., and Barth, J. A. C.: Acid rain footprint three decades after peak deposition: Long-term recovery from pollutant sulphate in the Uhlirska catchment (Czech Republic), The Science of the total environment, 598, 1037–1049,

865 doi:10.1016/j.scitotenv.2017.04.109, 2017b.

McGivney, E., Gustafsson, J. P., Belyazid, S., Zetterberg, T., and Löfgren, S.: Assessing the impact of acid rain and forest harvest intensity with the HD-MINTEQ model – soil chemistry of three Swedish conifer sites from 1880 to 2080, SOIL, 5, 63–77, doi:10.5194/soil-5-63-2019, 2019.

McGlynn, B. L. and McDonnell, J. J.: Quantifying the relative contributions of riparian and hillslope zones to catchment

870 runoff, Water Resour. Res., 39, 211, doi:10.1029/2003WR002091, 2003a.

McGlynn, B. L. and McDonnell, J. J.: Role of discrete landscape units in controlling catchment dissolved organic carbon dynamics, Water Resour. Res., 39, 251, doi:10.1029/2002WR001525, 2003b.

McGlynn, B. L. and Seibert, J.: Distributed assessment of contributing area and riparian buffering along stream networks, Water Resour. Res., 39, 331, doi:10.1029/2002WR001521, 2003.

875 McGuire, K. J. and McDonnell, J. J.: Hydrological connectivity of hillslopes and streams: Characteristic time scales and nonlinearities, Water Resour. Res., 46, 400, doi:10.1029/2010WR009341, 2010.

McNamara, J. P., Kane, D. L., and Hinzman, L. D.: Hydrograph separations in an arctic watershed using mixing model and graphical techniques, Water Resour. Res., 33, 1707–1719, doi:10.1029/97WR01033, 1997.

Meybeck, M.: Composition chimique des ruisseaux non pollués en France. Chemical composition of headwater streams in

880 France, sgeol, 39, 3–77, doi:10.3406/sgeol.1986.1719, 1986.

Meybeck, M.: Global chemical weathering of surficial rocks estimated from river dissolved loads, American Journal of Science, 287, 401–428, doi:10.2475/ajs.287.5.401, 1987.

Meyboom, P.: Groundwater Studies in the Assiboine River Drainage Basin. Part II: Hydrolofic Characteristics of Phreatophytic Vegetation in South-Central Saskatchewan, Geological Survey of Canada, Ottawa, Canada, 1967.

885 Michaelis, J.: Carbonate rock dissolution under intermediate system conditions, in: Progress in Hydrogeochemistry: Organics - Carbonate Systems - Silicate Systems - Microbiology - Models, Mattheß, G., Frimmel, F., Hirsch, P., Schulz, H. D., Usdowski, E. (Eds.), Springer Berlin Heidelberg, Berlin, Heidelberg, 167–174, 1992.

Michaelis, J., Usdowski, E., and Menschel, G.: Partitioning of 13 C and 12 C on the degassing of CO 2 and the precipitation of calcite; Rayleigh-type fractionation and a kinetic model, American Journal of Science, 285, 318–327, doi:10.2475/ajs.285.4.318, 1985.

Millero, F. J.: The thermodynamics of the carbonate system in seawater, Geochimica et Cosmochimica Acta, 43, 1651–1661, doi:10.1016/0016-7037(79)90184-4, 1979.

Millot, R., Gaillardet, J., Dupré, B., and Allègre, C. J.: The global control of silicate weathering rates and the coupling with physical erosion: new insights from rivers of the Canadian Shield, Earth and Planetary Science Letters, 196, 83–98, doi:10.1016/S0012-821X(01)00599-4, 2002.

Moore, J., Jacobson, A. D., Holmden, C., and Craw, D.: Tracking the relationship between mountain uplift, silicate weathering, and long-term CO2 consumption with Ca isotopes: Southern Alps, New Zealand, Chemical Geology, 341, 110–127, doi:10.1016/j.chemgeo.2013.01.005, 2013.

Moosdorf, N., Hartmann, J., and Lauerwald, R.: Changes in dissolved silica mobilization into river systems draining North America until the period 2081–2100, Journal of Geochemical Exploration, 110, 31–39, doi:10.1016/j.gexplo.2010.09.001, 2011.

Myrabø, S.: Temporal and spatial scale of response area and groundwater variation in Till, Hydrol. Process., 11, 1861–1880, doi:10.1002/(SICI)1099-1085(199711)11:14%3C1861:AID-HYP535%3E3.0.CO;2-P, 1997.

NGU: Berggrunn Data N250, Geological Survey of Norway, https://www.ngu.no/en/topic/datasets, 2022.

Obu, J., Westermann, S., Bartsch, A., Berdnikov, N., Christiansen, H. H., Dashtseren, A., Delaloye, R., Elberling, B., Etzelmüller, B., Kholodov, A., Khomutov, A., Kääb, A., Leibman, M. O., Lewkowicz, A. G., Panda, S. K., Romanovsky, V., Way, R. G., Westergaard-Nielsen, A., Wu, T., Yamkhin, J., and Zou, D.: Northern Hemisphere permafrost map based on TTOP modelling for 2000–2016 at 1 km2 scale, Earth-Science Reviews, 193, 299–316, doi:10.1016/j.earscirev.2019.04.023, 2019.

O'Leary, M. H.: Carbon Isotopes in Photosynthesis, BioScience, 38, 328–336, doi:10.2307/1310735, 1988.

Oliva, P., Dupré, B., Martin, F., and Viers, J.: The role of trace minerals in chemical weathering in a high-elevation granitic watershed (Estibère, France): Chemical and mineralogical evidence, Geochimica et Cosmochimica Acta, 68, 2223–2243, doi:10.1016/j.gca.2003.10.043, 2004.

Oliver, L., Harris, N., Bickle, M., Chapman, H., Dise, N., and Horstwood, M.: Silicate weathering rates decoupled from the 87Sr/86Sr ratio of the dissolved load during Himalayan erosion, Chemical Geology, 201, 119–139, doi:10.1016/S0009-2541(03)00236-5, 2003.

Olsen, L.: Stadials and interstadials during the Weichsel glackiation on Finnmarksvidda, northern Norway, Boreas, 17, 517–539, doi:10.1111/j.1502-3885.1988.tb00566.x, 1988.

Olsen, L., Fredin, O., and Olesen, O.: Quaternary Geology of Norway, Geological Survey of Norway Special Publication, 13, 2013.

O'Nions, R. K., Morton, R. D., and Batey, R.: Geological investigations in the Bamble sector of the Fennoscandian Shield South Norway.: I. The geology of eastern Bamble., Universitetsforlaget, Oslo, 1970.

Petrone, K. C., Hinzman, L. D., Shibata, H., Jones, J. B., and Boone, R. D.: The influence of fire and permafrost on sub-arctic stream chemistry during storms, Hydrol. Process., 21, 423–434, doi:10.1002/hyp.6247, 2007.

925 Pierrot, D. E., Wallace, D., and Lewis, E.: Carbon Dioxide Information Analysis Center, 2011.

Polsenaere, P. and Abril, G.: Modelling CO2 degassing from small acidic rivers using water pCO2, DIC and δ13C-DIC data, Geochimica et Cosmochimica Acta, 91, 220–239, doi:10.1016/j.gca.2012.05.030, 2012.

Porter, C., Morin, P., Howat, I., Noh, M.-J., Bates, B., Peterman, K., Keesey, S., Schlenk, M., Gardiner, J., Tomko, K., Willis, M., Kelleher, C., Cloutier, M., Husby, E., Foga, S., Nakamura, H., Platson, M., Wethington, M., JR., Williamson,
930 C., Bauer, G., Enos, J., Arnold, G., Kramer, W., Becker, P., Doshi, A., D'Souza, C., Cummens, P., Laurier, F., and Bojesen, M.: ArcticDEM, V1, Harvard Dataverse, 2018.

Purkamo, L., Ahn, C. M. E. von, Jilbert, T., Muniruzzaman, M., Bange, H. W., Jenner, A.-K., Böttcher, M. E., and Virtasalo, J. J.: Impact of submarine groundwater discharge on biogeochemistry and microbial communities in pockmarks, Geochimica et Cosmochimica Acta, 334, 14–44, doi:10.1016/j.gca.2022.06.040, 2022.

935 QGIS.org: QGIS Geographic Information System, QGIS Association, http://www.qgis.org, 2022.

Rantanen, M., Karpechko, A. Y., Lipponen, A., Nordling, K., Hyvärinen, O., Ruosteenoja, K., Vihma, T., and Laaksonen, A.: The Arctic has warmed nearly four times faster than the globe since 1979, Commun Earth Environ, 3, doi:10.1038/s43247-022-00498-3, 2022.

Raymond, P. A. and Hamilton, S. K.: Anthropogenic influences on riverine fluxes of dissolved inorganic carbon to the
940 oceans, Limnol Oceanogr Lett, 3, 143–155, doi:10.1002/lol2.10069, 2018.

Raymond, P. A., Oh, N.-H., Turner, R. E., and Broussard, W.: Anthropogenically enhanced fluxes of water and carbon from the Mississippi River, Nature, 451, 449–452, doi:10.1038/nature06505, 2008.

Riley, S. J., DeGloria, S. D., and and Elliot, R.: A terrain ruggedness index that quantifies topographic heterogeneity, Intermountain Journal of Sciences, 5, 23–27, 1999.

945 Rouault, E., Warmerdam, F., Schwehr, K., Kiselev, A., Butler, H., Łoskot, M., Szekeres, T., Tourigny, E., Landa, M., Miara, I., Elliston, B., Kumar, C., Plesea, L., Morissette, D., Jolma, A., and Dawson, N.: GDAL (v3.4.2), Zenodo, https://doi.org/10.5281/zenodo.6352176, 2022.

Sandström, B. and Tullborg, E.-L.: Episodic fluid migration in the Fennoscandian Shield recorded by stable isotopes, rare earth elements and fluid inclusions in fracture minerals at Forsmark, Sweden, Chemical Geology, 266, 126–142,
950 doi:10.1016/j.chemgeo.2009.04.019, 2009.

Schaefer, K. W. and Usdowski, E.: Models for the dissolution of carbonate rocks and the carbon-13/carbon-12 evolution of carbonate groundwaters, Zeitschrift fuer Wasser- und Abwasser-Forschung, 20, 69–81, 1987.

Schaefer, K. W. and Usdowski, E.: Application of stable carbon and sulfur isotope models to the development of ground water in a limestone-dolomite-anhydrite-gypsum area, in: Progress in Hydrogeochemistry: Organics - Carbonate

955   Systems - Silicate Systems - Microbiology - Models, Mattheß, G., Frimmel, F., Hirsch, P., Schulz, H. D., Usdowski, E. (Eds.), Springer Berlin Heidelberg, Berlin, Heidelberg, 157–163, 1992.

Seibert, J., Grabs, T., Köhler, S., Laudon, H., Winterdahl, M., and Bishop, K.: Linking soil- and stream-water chemistry based on a Riparian Flow-Concentration Integration Model, Hydrol. Earth Syst. Sci., 13, 2287–2297, doi:10.5194/hess-13-2287-2009, 2009.

960   Seklima: Observations and weather statistics, Norsk Klimaservicesenter, https://seklima.met.no/observations/, 2020.

Shadwick, E. H., Thomas, H., Gratton, Y., Leong, D., Moore, S. A., Papakyriakou, T., and Prowe, A.: Export of Pacific carbon through the Arctic Archipelago to the North Atlantic, Continental Shelf Research, 31, 806–816, doi:10.1016/j.csr.2011.01.014, 2011.

Shin, W. J., Chung, G. S., Lee, D., and Lee, K. S.: Dissolved inorganic carbon export from carbonate and silicate catchments 965   estimated from carbonate chemistry and $\delta^{13}C_{DIC}$, Hydrol. Earth Syst. Sci., 15, 2551–2560, doi:10.5194/hess-15-2551-2011, 2011.

Sollid, J. L., Andersen, S., Hamre, N., Kjeldsen, O., Salvigsen, O., Sturød, S., Tveitå, T., and Wilhelmsen, A.: Deglaciation of Finnmark, North Norway, Norsk Geografisk Tidsskrift - Norwegian Journal of Geography, 27, 233–325, doi:10.1080/00291951.1973.9728306, 1973.

970   Stallard, R. F. and Edmond, J. M.: Geochemistry of the Amazon: 3. Weathering chemistry and limits to dissolved inputs, J. Geophys. Res., 92, 8293, doi:10.1029/JC092iC08p08293, 1987.

Stone, L. E., Fang, X., Haynes, K. M., Helbig, M., Pomeroy, J. W., Sonnentag, O., and Quinton, W. L.: Modelling the effects of permafrost loss on discharge from a wetland-dominated, discontinuous permafrost basin, Hydrol. Process., 33, 2607–2626, doi:10.1002/hyp.13546, 2019.

975   Striegl, R. G., Aiken, G. R., Dornblaser, M. M., Raymond, P. A., and Wickland, K. P.: A decrease in discharge-normalized DOC export by the Yukon River during summer through autumn, Geophys. Res. Lett., 32, 567, doi:10.1029/2005GL024413, 2005.

Stroeven, A. P., Hättestrand, C., Kleman, J., Heyman, J., Fabel, D., Fredin, O., Goodfellow, B. W., Harbor, J. M., Jansen, J. D., Olsen, L., Caffee, M. W., Fink, D., Lundqvist, J., Rosqvist, G. C., Strömberg, B., and Jansson, K. N.: Deglaciation of 980   Fennoscandia, Quaternary Science Reviews, 147, 91–121, doi:10.1016/j.quascirev.2015.09.016, 2016.

Stumm, W. and Morgan, J. J.: Aquatic chemistry an introduction chemical equilibria in natural water, 2nd ed., A Wiley - Interscience Publication, A Wiley-Interscience Publication, New York, 780 pp., 1981.

Tank, S. E., Frey, K. E., Striegl, R. G., Raymond, P. A., Holmes, R. M., McClelland, J. W., and Peterson, B. J.: Landscape-level controls on dissolved carbon flux from diverse catchments of the circumboreal, Global Biogeochem. Cycles, 26, 985   323, doi:10.1029/2012GB004299, 2012.

Tanneberger, F., Tegetmeyer, C., Busse, S., Barthelmes, A., and and 55 others: The peatland map of Europe, Mires and Peat, 19, 1–17, doi:10.19189/MaP.2016.OMB.264, 2017.

Trolier, M., White, J. W. C., Tans, P. P., Masarie, K. A., and Gemery, P. A.: Monitoring the isotopic composition of atmospheric CO 2: Measurements from the NOAA Global Air Sampling Network, J. Geophys. Res., 101, 25897–25916, doi:10.1029/96JD02363, 1996.

Vidon, P.: Towards a better understanding of riparian zone water table response to precipitation: Surface water infiltration, hillslope contribution or pressure wave processes?, Hydrol. Process., 26, 3207–3215, doi:10.1002/hyp.8258, 2012.

Walker, J. C. G., Hays, P. B., and Kasting, J. F.: A negative feedback mechanism for the long-term stabilization of Earth's surface temperature, J. Geophys. Res., 86, 9776, doi:10.1029/JC086iC10p09776, 1981.

Walvoord, M. A. and Striegl, R. G.: Increased groundwater to stream discharge from permafrost thawing in the Yukon River basin: Potential impacts on lateral export of carbon and nitrogen, Geophys. Res. Lett., 34, L19401, doi:10.1029/2007GL030216, 2007.

Warner, D. L., Bond-Lamberty, B., Jian, J., Stell, E., and Vargas, R.: Spatial Predictions and Associated Uncertainty of Annual Soil Respiration at the Global Scale, Global Biogeochem. Cycles, 33, 1733–1745, doi:10.1029/2019GB006264, 2019.

Watts, J. D., Natali, S. M., Minions, C., Risk, D., Arndt, K., Zona, D., Euskirchen, E. S., Rocha, A. V., Sonnentag, O., Helbig, M., Kalhori, A., Oechel, W., Ikawa, H., Ueyama, M., Suzuki, R., Kobayashi, H., Celis, G., Schuur, E. A. G., Humphreys, E., Kim, Y., Lee, B.-Y., Goetz, S., Madani, N., Schiferl, L. D., Commane, R., Kimball, J. S., Liu, Z., Torn, M. S., Potter, S., Wang, J. A., Jorgenson, M. T., Xiao, J., Li, X., and Edgar, C.: Soil respiration strongly offsets carbon uptake in Alaska and Northwest Canada, Environ. Res. Lett., 16, 84051, doi:10.1088/1748-9326/ac1222, 2021.

White, A. F., Bullen, T. D., Vivit, D. V., Schulz, M. S., and Clow, D. W.: The role of disseminated calcite in the chemical weathering of granitoid rocks, Geochimica et Cosmochimica Acta, 63, 1939–1953, doi:10.1016/S0016-7037(99)00082-4, 1999.

White, A. F., Schulz, M. S., Lowenstern, J. B., Vivit, D. V., and Bullen, T. D.: The ubiquitous nature of accessory calcite in granitoid rocks: Implications for weathering, solute evolution, and petrogenesis, Geochimica et Cosmochimica Acta, 69, 1455–1471, doi:10.1016/j.gca.2004.09.012, 2005.

Winde, V., Böttcher, M. E., Escher, P., Böning, P., Beck, M., Liebezeit, G., and Schneider, B.: Tidal and spatial variations of DI13C and aquatic chemistry in a temperate tidal basin during winter time, Journal of Marine Systems, 129, 396–404, doi:10.1016/j.jmarsys.2013.08.005, 2014.

Yuanrong, S., Ruihong, Y., Mingyang, T., Xiankun, Y., Lishan, R., Haizhu, H., Zhuangzhuang, Z., and Xixi, L.: Major ion chemistry in the headwater region of the Yellow River: Impact of land covers, Environ Earth Sci, 80, 2637, doi:10.1007/s12665-021-09692-6, 2021.

Zeebe, R. E. and Westbroek, P.: A simple model for the CaCO 3 saturation state of the ocean: The "Strangelove," the "Neritan," and the "Cretan" Ocean, Geochem. Geophys. Geosyst., 4, doi:10.1029/2003GC000538, 2003.

1020   Zeng, S., Kaufmann, G., and Liu, Z.: Natural and Anthropogenic Driving Forces of Carbonate Weathering and the Related Carbon Sink Flux: A Model Comparison Study at Global Scale, Global Biogeochem. Cycles, 36, 46, doi:10.1029/2021GB007096, 2022.

Zeng, S., Liu, Z., and Kaufmann, G.: Sensitivity of the global carbonate weathering carbon-sink flux to climate and land-use changes, Nature communications, 10, 5749, doi:10.1038/s41467-019-13772-4, 2019.

1025   Zhang, J., Quay, P. D., and Wilbur, D. O.: Carbon isotope fractionation during gas-water exchange and dissolution of CO2, Geochimica et Cosmochimica Acta, 59, 107–114, doi:10.1016/0016-7037(95)91550-D, 1995.

Zolkos, S., Tank, S. E., Striegl, R. G., Kokelj, S. V., Kokoszka, J., Estop-Aragonés, C., and Olefeldt, D.: Thermokarst amplifies fluvial inorganic carbon cycling and export across watershed scales on the Peel Plateau, Canada, Biogeosciences, 17, 5163–5182, doi:10.5194/bg-17-5163-2020, 2020.

1030